

## 17

## Aperture Antennas

## 17.1 Open-Ended Waveguides

The aperture fields over an open-ended waveguide are not uniform over the aperture. The standard assumption is that they are equal to the fields that would exist if the guide were to be continued [1].

Fig. 17.1.1 shows a waveguide aperture of dimensions  $a > b$ . Putting the origin in the middle of the aperture, we assume that the tangential aperture fields  $E_a$ ,  $H_a$  are equal to those of the  $TE_{10}$  mode. We have from Eq. (8.4.3):

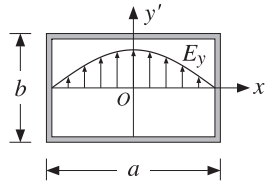


Fig. 17.1.1 Electric field over a waveguide aperture.

$$E_y(x') = E_0 \cos\left(\frac{\pi x'}{a}\right), \quad H_x(x') = -\frac{1}{\eta_{TE}} E_0 \cos\left(\frac{\pi x'}{a}\right) \quad (17.1.1)$$

where  $\eta_{TE} = \eta/K$  with  $K = \sqrt{1 - \omega_c^2/\omega^2} = \sqrt{1 - (\lambda/2a)^2}$ . Note that the boundary conditions are satisfied at the left and right walls,  $x' = \pm a/2$ .

For larger apertures, such as  $a > 2\lambda$ , we may set  $K \approx 1$ . For smaller apertures, such as  $0.5\lambda \leq a \leq 2\lambda$ , we will work with the generalized Huygens source condition (16.5.7). The radiated fields are given by Eq. (16.5.5), with  $f_x = 0$ :

$$\begin{aligned} E_\theta &= jk \frac{e^{-jkr}}{2\pi r} c_\theta f_y(\theta, \phi) \sin \phi \\ E_\phi &= jk \frac{e^{-jkr}}{2\pi r} c_\phi f_y(\theta, \phi) \cos \phi \end{aligned} \quad (17.1.2)$$

where  $f_y(\theta, \phi)$  is the aperture Fourier transform of  $E_y(x')$ , that is,

$$\begin{aligned} f_y(\theta, \phi) &= \int_{-a/2}^{a/2} \int_{-b/2}^{b/2} E_y(x') e^{jk_x x' + jk_y y'} dx' dy' \\ &= E_0 \int_{-a/2}^{a/2} \cos\left(\frac{\pi x'}{a}\right) e^{jk_x x'} dx' \cdot \int_{-b/2}^{b/2} e^{jk_y y'} dy' \end{aligned}$$

The  $y'$ -integration is the same as that for a uniform line aperture. For the  $x'$ -integration, we use the definite integral:

$$\int_{-a/2}^{a/2} \cos\left(\frac{\pi x'}{a}\right) e^{jk_x x'} dx' = \frac{2a}{\pi} \frac{\cos(k_x a/2)}{1 - (k_x a/\pi)^2}$$

It follows that:

$$f_y(\theta, \phi) = E_0 \frac{2ab}{\pi} \frac{\cos(\pi v_x)}{1 - 4v_x^2} \frac{\sin(\pi v_y)}{\pi v_y} \quad (17.1.3)$$

where  $v_x = k_x a/2\pi$  and  $v_y = k_y b/2\pi$ , or,

$$v_x = \frac{a}{\lambda} \sin \theta \cos \phi, \quad v_y = \frac{b}{\lambda} \sin \theta \sin \phi \quad (17.1.4)$$

The obliquity factors can be chosen to be one of the three cases: (a) the PEC case, if the aperture is terminated in a ground plane, (b) the ordinary Huygens source case, if it is radiating into free space, or (c) the modified Huygens source case. Thus,

$$\begin{bmatrix} c_\theta \\ c_\phi \end{bmatrix} = \begin{bmatrix} 1 \\ \cos \theta \end{bmatrix}, \quad \frac{1}{2} \begin{bmatrix} 1 + \cos \theta \\ 1 + \cos \theta \end{bmatrix}, \quad \frac{1}{2} \begin{bmatrix} 1 + K \cos \theta \\ K + \cos \theta \end{bmatrix} \quad (17.1.5)$$

By normalizing all three cases to unity at  $\theta = 0^\circ$ , we may combine them into:

$$c_E(\theta) = \frac{1 + K \cos \theta}{1 + K}, \quad c_H(\theta) = \frac{K + \cos \theta}{1 + K} \quad (17.1.6)$$

where  $K$  is one of the three possible values:

$$K = 0, \quad K = 1, \quad K = \frac{\eta}{\eta_{TE}} = \sqrt{1 - \left(\frac{\lambda}{2a}\right)^2} \quad (17.1.7)$$

The *normalized gains* along the two principal planes are given as follows. For the  $xz$ - or the  $H$ -plane, we set  $\phi = 0^\circ$ , which gives  $E_\theta = 0$ :

$$g_H(\theta) = \frac{|E_\phi(\theta)|^2}{|E_\phi|_{\max}^2} = |c_H(\theta)|^2 \left| \frac{\cos(\pi v_x)}{1 - 4v_x^2} \right|^2, \quad v_x = \frac{a}{\lambda} \sin \theta \quad (17.1.8)$$

And, for the  $yz$ - or  $E$ -plane, we set  $\phi = 90^\circ$ , which gives  $E_\phi = 0$ :

$$g_E(\theta) = \frac{|E_\theta(\theta)|^2}{|E_\theta|_{\max}^2} = |c_E(\theta)|^2 \left| \frac{\sin(\pi v_y)}{\pi v_y} \right|^2, \quad v_y = \frac{b}{\lambda} \sin \theta \quad (17.1.9)$$

The function  $\cos(\pi v_x) / (1 - 4v_x^2)$  determines the essential properties of the  $H$ -plane pattern. It is essentially a double-sinc function, as can be seen from the identity:

$$\frac{\cos(\pi v_x)}{1 - 4v_x^2} = \frac{\pi}{4} \left[ \frac{\sin\left(\pi\left(v_x + \frac{1}{2}\right)\right)}{\pi\left(v_x + \frac{1}{2}\right)} + \frac{\sin\left(\pi\left(v_x - \frac{1}{2}\right)\right)}{\pi\left(v_x - \frac{1}{2}\right)} \right] \quad (17.1.10)$$

It can be evaluated with the help of the MATLAB function `dsinc`, with usage:

$$y = \text{dsinc}(x); \quad \% \text{ the double-sinc function } \frac{\cos(\pi x)}{1 - 4x^2} = \frac{\pi}{4} [\text{sinc}(x + 0.5) + \text{sinc}(x - 0.5)]$$

The 3-dB width of the  $E$ -plane pattern is the same as for the uniform rectangular aperture,  $\Delta\theta_y = 0.886 \lambda/b$ . The `dsinc` function has the value  $\pi/4$  at  $v_x = 1/2$ . Its 3-dB point is at  $v_x = 0.5945$ , its first null at  $v_x = 1.5$ , and its first sidelobe at  $v_x = 1.8894$  and has height 0.0708 or 23 dB down from the main lobe. It follows from  $v_x = a \sin \theta / \lambda$  that the 3-dB width in angle space will be  $\Delta\theta_x = 2 \times 0.5945 \lambda/a = 1.189 \lambda/a$ . Thus, the 3-dB widths are in radians and in degrees:

$$\Delta\theta_x = 1.189 \frac{\lambda}{a} = 68.12^\circ \frac{\lambda}{a}, \quad \Delta\theta_y = 0.886 \frac{\lambda}{b} = 50.76^\circ \frac{\lambda}{b} \quad (17.1.11)$$

**Example 17.1.1:** Fig. 17.1.2 shows the  $H$ - and  $E$ -plane patterns for a WR90 waveguide operating at 10 GHz, so that  $\lambda = 3$  cm. The guide dimensions are  $a = 2.282$  cm,  $b = 1.016$  cm. The typical MATLAB code for generating these graphs was:

```
a = 2.282; b = 1.016; la = 3;
th = (0:0.5:90) * pi/180;
vx = a/la * sin(th);
vy = b/la * sin(th);
K = sqrt(1 - (la/(2*a))^2); % alternatively, K = 0, or, K = 1
cE = (1 + K*cos(th))/(K+1); % normalized obliquity factors
cH = (K + cos(th))/(K+1);
gH = abs(cH .* dsinc(vx).^2); % uses dsinc
gE = abs(cE .* sinc(vy).^2); % uses sinc from SP toolbox
figure; dbp(th,gH,45,12); % dB gain polar plot
figure; dbp(th,gE,45,12);
```

The three choices of obliquity factors have been plotted for comparison. We note that the Huygens source cases,  $K = 1$  and  $K = \eta/\eta_{TE}$ , differ very slightly. The  $H$ -plane pattern vanishes at  $\theta = 90^\circ$  in the PEC case ( $K = 0$ ), but not in the Huygens source cases.

The gain computed from Eq. (17.1.13) is  $G = 2.62$  or 4.19 dB, and computed from Eq. (17.1.14),  $G = 2.67$  or 4.28 dB, where  $K = \eta/\eta_{TE} = 0.75$  and  $(K + 1)^2/4K = 1.02$ .

This waveguide is not a high-gain antenna. Increasing the dimensions  $a, b$  is impractical and also would allow the propagation of higher modes, making it very difficult to restrict operation to the  $TE_{10}$  mode.  $\square$

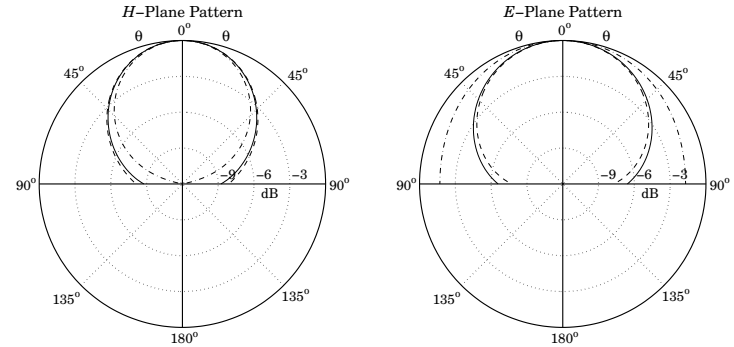


Fig. 17.1.2 Solid line has  $K = \eta/\eta_{TE}$ , dashed,  $K = 1$ , and dash-dotted,  $K = 0$ .

Next, we derive an expression for the directivity and gain of the waveguide aperture. The maximum intensity is obtained at  $\theta = 0^\circ$ . Because  $c_\theta(0) = c_\phi(0)$ , we have:

$$U_{\max} = \frac{1}{2\eta} |E(0, \phi)|^2 = \frac{1}{2\lambda^2\eta} c_\theta^2(0) |f_y(0, \phi)|^2 = \frac{1}{2\lambda^2\eta} c_\theta^2(0) |E_0|^2 \frac{4(ab)^2}{\pi^2}$$

The total power transmitted through the aperture and radiated away is the power propagated down the waveguide given by Eq. (8.7.4), that is,

$$P_{\text{rad}} = \frac{1}{4\eta_{TE}} |E_0|^2 ab \quad (17.1.12)$$

It follows that the gain/directivity of the aperture will be:

$$G = 4\pi \frac{U_{\max}}{P_{\text{rad}}} = \frac{4\pi}{\lambda^2} \frac{8}{\pi^2} (ab) \frac{\eta_{TE}}{\eta} c_\theta^2(0)$$

For the PEC and ordinary Huygens cases,  $c_\theta(0) = 1$ . Assuming  $\eta_{TE} \approx \eta$ , we have:

$$G = \frac{4\pi}{\lambda^2} \frac{8}{\pi^2} (ab) = 0.81 \frac{4\pi}{\lambda^2} (ab) \quad (17.1.13)$$

Thus, the effective area of the waveguide aperture is  $A_{\text{eff}} = 0.81(ab)$  and the aperture efficiency  $e = 0.81$ . For the modified Huygens case, we have for the obliquity factor  $c_\theta(0) = (K + 1)/2$  with  $K = \eta/\eta_{TE}$ . It follows that [745]:

$$G = \frac{4\pi}{\lambda^2} \frac{8}{\pi^2} (ab) \frac{(K + 1)^2}{4K} \quad (17.1.14)$$

For waveguides larger than about a wavelength, the directivity factor  $(K + 1)^2/4K$  is practically equal to unity, and the directivity is accurately given by Eq. (17.1.13). The table below shows some typical values of  $K$  and the directivity factor (operation in the  $TE_{10}$  mode requires  $0.5\lambda < a < \lambda$ ):

$a/\lambda$	$K$	$(K + 1)^2 / (4K)$
0.6	0.5528	1.0905
0.8	0.7806	1.0154
1.0	0.8660	1.0052
1.5	0.9428	1.0009
2.0	0.9682	1.0003

The gain-beamwidth product is from Eqs. (17.1.11) and (17.1.13),  $p = G \Delta\theta_x \Delta\theta_y = 4\pi (0.81) (0.886) (1.189) = 10.723 \text{ rad}^2 = 35\,202 \text{ deg}^2$ . Thus, another instance of the general formula (14.3.14) is (with the angles given in radians and in degrees):

$$G = \frac{10.723}{\Delta\theta_x \Delta\theta_y} = \frac{35\,202}{\Delta\theta_x^\circ \Delta\theta_y^\circ} \tag{17.1.15}$$

### 17.2 Horn Antennas

The only practical way to increase the directivity of a waveguide is to flare out its ends into a horn. Fig. 17.2.1 shows three types of horns: The *H*-plane sectoral horn in which the long side of the waveguide (the *a*-side) is flared, the *E*-plane sectoral horn in which the short side is flared, and the pyramidal horn in which both sides are flared.

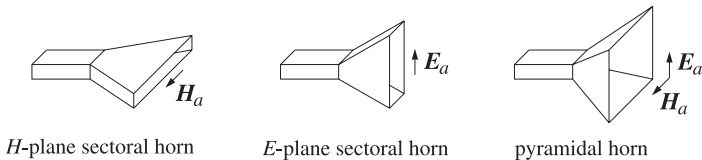


Fig. 17.2.1 *H*-plane, *E*-plane, and pyramidal horns.

The pyramidal horn is the most widely used antenna for feeding large microwave dish antennas and for calibrating them. The sectoral horns may be considered as special limits of the pyramidal horn. We will discuss only the pyramidal case.

Fig. 17.2.2 shows the geometry in more detail. The two lower figures are the cross-sectional views along the *xz*- and *yz*-planes. It follows from the geometry that the various lengths and flare angles are given by:

$$\begin{aligned} R_a &= \frac{A}{A-a} R_A, & R_b &= \frac{B}{B-b} R_B \\ L_a^2 &= R_a^2 + \frac{A^2}{4}, & L_b^2 &= R_b^2 + \frac{B^2}{4} \\ \tan \alpha &= \frac{A}{2R_a}, & \tan \beta &= \frac{B}{2R_b} \\ \Delta_a &= \frac{A^2}{8R_a}, & \Delta_b &= \frac{B^2}{8R_b} \end{aligned} \tag{17.2.1}$$

The quantities  $R_A$  and  $R_B$  represent the perpendicular distances from the plane of the waveguide opening to the plane of the horn. Therefore, they must be *equal*,  $R_A = R_B$ . Given the horn sides  $A, B$  and the common length  $R_A$ , Eqs. (17.2.1) allow the calculation of all the relevant geometrical quantities required for the construction of the horn.

The lengths  $\Delta_a$  and  $\Delta_b$  represent the maximum deviation of the radial distance from the plane of the horn. The expressions given in Eq. (17.2.1) are approximations obtained when  $R_a \gg A$  and  $R_b \gg B$ . Indeed, using the small- $x$  expansion,

$$\sqrt{1 \pm x} \approx 1 \pm \frac{x}{2}$$

we have two possible ways to approximate  $\Delta_a$ :

$$\begin{aligned} \Delta_a &= L_a - R_a = \sqrt{R_a^2 + \frac{A^2}{4}} - R_a = R_a \sqrt{1 + \frac{A^2}{4R_a^2}} - R_a \approx \frac{A^2}{8R_a} \\ &= L_a - \sqrt{L_a^2 - \frac{A^2}{4}} = L_a - L_a \sqrt{1 - \frac{A^2}{4L_a^2}} \approx \frac{A^2}{8L_a} \end{aligned} \tag{17.2.2}$$

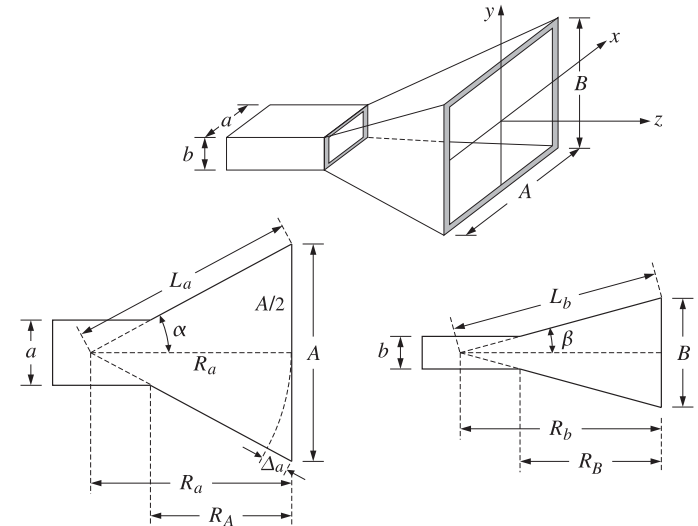


Fig. 17.2.2 The geometry of the pyramidal horn requires  $R_A = R_B$ .

The two expressions are equal to within the assumed approximation order. The length  $\Delta_a$  is the maximum deviation of the radial distance at the edge of the horn plane, that is, at  $x = \pm A/2$ . For any other distance  $x$  along the *A*-side of the horn, and distance  $y$  along the *B*-side, the deviations will be:

$$\Delta_a(x) = \frac{x^2}{2R_a}, \quad \Delta_b(y) = \frac{y^2}{2R_b} \tag{17.2.3}$$

The quantities  $k\Delta_a(x)$  and  $k\Delta_b(y)$  are the relative phase differences at the point  $(x, y)$  on the aperture of the horn relative to the center of the aperture. To account for these phase differences, the aperture electric field is assumed to have the form:

$$E_y(x, y) = E_0 \cos\left(\frac{\pi x}{A}\right) e^{-jk\Delta_a(x)} e^{-jk\Delta_b(y)}, \quad \text{or,} \quad (17.2.4)$$

$$E_y(x, y) = E_0 \cos\left(\frac{\pi x}{A}\right) e^{-jkx^2/2R_a} e^{-jky^2/2R_b} \quad (17.2.5)$$

We note that at the connecting end of the waveguide the electric field is  $E_y(x, y) = E_0 \cos(\pi x/A)$  and changes gradually into the form of Eq. (17.2.5) at the horn end.

Because the aperture sides  $A, B$  are assumed to be large compared to  $\lambda$ , the Huygens source assumption is fairly accurate for the tangential aperture magnetic field,  $H_x(x, y) = -E_y(x, y)/\eta$ , so that:

$$H_x(x, y) = -\frac{1}{\eta} E_0 \cos\left(\frac{\pi x}{A}\right) e^{-jkx^2/2R_a} e^{-jky^2/2R_b} \quad (17.2.6)$$

The quantities  $k\Delta_a, k\Delta_b$  are the maximum phase deviations in radians. Therefore,  $\Delta_a/\lambda$  and  $\Delta_b/\lambda$  will be the maximum deviations in cycles. We define:

$$S_a = \frac{\Delta_a}{\lambda} = \frac{A^2}{8\lambda R_a}, \quad S_b = \frac{\Delta_b}{\lambda} = \frac{B^2}{8\lambda R_b} \quad (17.2.7)$$

It turns out that the optimum values of these parameters that result into the highest directivity are approximately:  $S_a = 3/8$  and  $S_b = 1/4$ . We will use these values later in the design of optimum horns. For the purpose of deriving convenient expressions for the radiation patterns of the horn, we define the related quantities:

$$\sigma_a^2 = 4S_a = \frac{A^2}{2\lambda R_a}, \quad \sigma_b^2 = 4S_b = \frac{B^2}{2\lambda R_b} \quad (17.2.8)$$

The near-optimum values of these constants are  $\sigma_a = \sqrt{4S_a} = \sqrt{4(3/8)} = 1.2247$  and  $\sigma_b = \sqrt{4S_b} = \sqrt{4(1/4)} = 1$ . These are used very widely, but they are not quite the true optimum values, which are  $\sigma_a = 1.2593$  and  $\sigma_b = 1.0246$ .

Replacing  $k = 2\pi/\lambda$  and  $2\lambda R_a = A^2/\sigma_a^2$  and  $2\lambda R_b = B^2/\sigma_b^2$  in Eq. (17.2.5), we may rewrite the aperture fields in the form: For  $-A/2 \leq x \leq A/2$  and  $-B/2 \leq y \leq B/2$ ,

$$\begin{aligned} E_y(x, y) &= E_0 \cos\left(\frac{\pi x}{A}\right) e^{-j(\pi/2)\sigma_a^2(2x/A)^2} e^{-j(\pi/2)\sigma_b^2(2y/B)^2} \\ H_x(x, y) &= -\frac{1}{\eta} E_0 \cos\left(\frac{\pi x}{A}\right) e^{-j(\pi/2)\sigma_a^2(2x/A)^2} e^{-j(\pi/2)\sigma_b^2(2y/B)^2} \end{aligned} \quad (17.2.9)$$

### 17.3 Horn Radiation Fields

As in the case of the open-ended waveguide, the aperture Fourier transform of the electric field has only a  $y$ -component given by:

$$\begin{aligned} f_y(\theta, \phi) &= \int_{-A/2}^{A/2} \int_{-B/2}^{B/2} E_y(x, y) e^{jk_x x + jk_y y} dx dy \\ &= E_0 \int_{-A/2}^{A/2} \cos\left(\frac{\pi x}{A}\right) e^{jk_x x} e^{-j(\pi/2)\sigma_a^2(2x/A)^2} dx \cdot \int_{-B/2}^{B/2} e^{jk_y y} e^{-j(\pi/2)\sigma_b^2(2y/B)^2} dy \end{aligned}$$

The above integrals can be expressed in terms of the following diffraction-like integrals, whose properties are discussed in Appendix F:

$$\begin{aligned} F_0(\nu, \sigma) &= \int_{-1}^1 e^{j\pi\nu\xi} e^{-j(\pi/2)\sigma^2\xi^2} d\xi \\ F_1(\nu, \sigma) &= \int_{-1}^1 \cos\left(\frac{\pi\xi}{2}\right) e^{j\pi\nu\xi} e^{-j(\pi/2)\sigma^2\xi^2} d\xi \end{aligned} \quad (17.3.1)$$

The function  $F_0(\nu, \sigma)$  can be expressed as:

$$F_0(\nu, \sigma) = \frac{1}{\sigma} e^{j(\pi/2)(\nu^2/\sigma^2)} \left[ F\left(\frac{\nu}{\sigma} + \sigma\right) - F\left(\frac{\nu}{\sigma} - \sigma\right) \right] \quad (17.3.2)$$

where  $F(x) = C(x) - jS(x)$  is the standard Fresnel integral, discussed in Appendix F. Then, the function  $F_1(\nu, \sigma)$  can be expressed in terms of  $F_0(\nu, \sigma)$ :

$$F_1(\nu, \sigma) = \frac{1}{2} [F_0(\nu + 0.5, \sigma) + F_0(\nu - 0.5, \sigma)] \quad (17.3.3)$$

The functions  $F_0(\nu, \sigma)$  and  $F_1(\nu, \sigma)$  can be evaluated numerically for any vector of values  $\nu$  and any positive scalar  $\sigma$  (including  $\sigma = 0$ ) using the MATLAB function `diffint`, which is further discussed in Appendix F and has usage:

```
F0 = diffint(v, sigma, 0); % evaluates the function Fb0(v, sigma)
F1 = diffint(v, sigma, 1); % evaluates the function Fb1(v, sigma)
```

In addition to `diffint`, the following MATLAB functions, to be discussed later, facilitate working with horn antennas:

```
hband % calculate 3-dB bandedges
heff % calculate aperture efficiency
hgain % calculate H- and E-plane gains
hopt % optimum horn design
hsigma % calculate optimum values of sigma_b, sigma_b
```

Next, we express the radiation patterns in terms of the functions (17.3.1). Defining the normalized wavenumbers  $\nu_x = k_x A/2\pi$  and  $\nu_y = k_y B/2\pi$ , we have:

$$\nu_x = \frac{A}{\lambda} \sin\theta \cos\phi, \quad \nu_y = \frac{B}{\lambda} \sin\theta \sin\phi \quad (17.3.4)$$

Changing variables to  $\xi = 2y/B$ , the  $y$ -integral can be written in terms of  $F_0(\nu, \sigma)$ :

$$\int_{-B/2}^{B/2} e^{jk_y y} e^{-j(\pi/2)\sigma_b^2(2y/B)^2} dy = \frac{B}{2} \int_{-1}^1 e^{j\pi v_y \xi} e^{-j(\pi/2)\sigma_b^2 \xi^2} d\xi = \frac{B}{2} F_0(v_y, \sigma_b)$$

Similarly, changing variables to  $\xi = 2x/A$ , we find for the  $x$ -integral:

$$\begin{aligned} \int_{-A/2}^{A/2} \cos\left(\frac{\pi x}{A}\right) e^{jk_x x} e^{-j(\pi/2)\sigma_a^2(2x/A)^2} dx \\ = \frac{A}{2} \int_{-1}^1 \cos\left(\frac{\pi \xi}{2}\right) e^{j\pi v_x \xi} e^{-j(\pi/2)\sigma_a^2 \xi^2} d\xi = \frac{A}{2} F_1(v_x, \sigma_a) \end{aligned}$$

It follows that the Fourier transform  $f_y(\theta, \phi)$  will be:

$$f_y(\theta, \phi) = E_0 \frac{AB}{4} F_1(v_x, \sigma_a) F_0(v_y, \sigma_b) \quad (17.3.5)$$

The open-ended waveguide and the sectoral horns can be thought of as limiting cases of Eq. (17.3.5), as follows:

1. open-ended waveguide:  $\sigma_a = 0$ ,  $A = a$ ,  $\sigma_b = 0$ ,  $B = b$ .
2.  $H$ -plane sectoral horn:  $\sigma_a > 0$ ,  $A > a$ ,  $\sigma_b = 0$ ,  $B = b$ .
3.  $E$ -plane sectoral horn:  $\sigma_a = 0$ ,  $A = a$ ,  $\sigma_b > 0$ ,  $B > b$ .

In these cases, the  $F$ -factors with  $\sigma = 0$  can be replaced by the following simplified forms, which follow from equations (F.12) and (F.17) of Appendix F:

$$F_0(v_y, 0) = 2 \frac{\sin(\pi v_y)}{\pi v_y}, \quad F_1(v_x, 0) = \frac{4}{\pi} \frac{\cos(\pi v_x)}{1 - 4v_x^2} \quad (17.3.6)$$

The radiation fields are obtained from Eq. (16.5.5), with obliquity factors  $c_\theta(\theta) = c_\phi(\theta) = (1 + \cos \theta)/2$ . Replacing  $k = 2\pi/\lambda$ , we have:

$$\begin{aligned} E_\theta &= j \frac{e^{-jkr}}{\lambda r} c_\theta(\theta) f_y(\theta, \phi) \sin \phi \\ E_\phi &= j \frac{e^{-jkr}}{\lambda r} c_\phi(\theta) f_y(\theta, \phi) \cos \phi \end{aligned} \quad (17.3.7)$$

or, explicitly,

$$\begin{aligned} E_\theta &= j \frac{e^{-jkr}}{\lambda r} E_0 \frac{AB}{4} \left( \frac{1 + \cos \theta}{2} \right) \sin \phi F_1(v_x, \sigma_a) F_0(v_y, \sigma_b) \\ E_\phi &= j \frac{e^{-jkr}}{\lambda r} E_0 \frac{AB}{4} \left( \frac{1 + \cos \theta}{2} \right) \cos \phi F_1(v_x, \sigma_a) F_0(v_y, \sigma_b) \end{aligned} \quad (17.3.8)$$

### Horn Radiation Patterns

The radiation intensity is  $U(\theta, \phi) = r^2(|E_\theta|^2 + |E_\phi|^2)/2\eta$ , so that:

$$U(\theta, \phi) = \frac{1}{32\eta\lambda^2} |E_0|^2 (AB)^2 c_\theta^2(\theta) |F_1(v_x, \sigma_a) F_0(v_y, \sigma_b)|^2 \quad (17.3.9)$$

Assuming that the maximum intensity is towards the forward direction, that is, at  $v_x = v_y = 0$ , we have:

$$U_{\max} = \frac{1}{32\eta\lambda^2} |E_0|^2 (AB)^2 |F_1(0, \sigma_a) F_0(0, \sigma_b)|^2 \quad (17.3.10)$$

The direction of maximum gain is not necessarily in the forward direction, but it may be nearby. This happens typically when  $\sigma_b > 1.54$ . Most designs use the optimum value  $\sigma_b = 1$ , which does have a maximum in the forward direction. With these caveats in mind, we define the *normalized gain*:

$$g(\theta, \phi) = \frac{U(\theta, \phi)}{U_{\max}} = \left| \frac{1 + \cos \theta}{2} \right|^2 \left| \frac{F_1(v_x, \sigma_a) F_0(v_y, \sigma_b)}{F_1(0, \sigma_a) F_0(0, \sigma_b)} \right|^2 \quad (17.3.11)$$

Similarly, the  $H$ - and  $E$ -plane gains corresponding to  $\phi = 0^\circ$  and  $\phi = 90^\circ$  are:

$$g_H(\theta) = \left| \frac{1 + \cos \theta}{2} \right|^2 \left| \frac{F_1(v_x, \sigma_a)}{F_1(0, \sigma_a)} \right|^2 = g(\theta, 0^\circ), \quad v_x = \frac{A}{\lambda} \sin \theta \quad (17.3.12)$$

$$g_E(\theta) = \left| \frac{1 + \cos \theta}{2} \right|^2 \left| \frac{F_0(v_y, \sigma_b)}{F_0(0, \sigma_b)} \right|^2 = g(\theta, 90^\circ), \quad v_y = \frac{B}{\lambda} \sin \theta$$

The normalizing values  $F_1(0, \sigma_a)$  and  $F_0(0, \sigma_b)$  are obtained from Eqs. (F.11) and (F.15) of Appendix F. They are given in terms of the Fresnel function  $F(x) = C(x) - jS(x)$  as follows:

$$\begin{aligned} |F_1(0, \sigma_a)|^2 &= \frac{1}{\sigma_a^2} \left| F\left(\frac{1}{2\sigma_a} + \sigma_a\right) - F\left(\frac{1}{2\sigma_a} - \sigma_a\right) \right|^2 \\ |F_0(0, \sigma_b)|^2 &= 4 \left| \frac{F(\sigma_b)}{\sigma_b} \right|^2 \end{aligned} \quad (17.3.13)$$

These have the limiting values for  $\sigma_a = 0$  and  $\sigma_b = 0$ :

$$|F_1(0, 0)|^2 = \frac{16}{\pi^2}, \quad |F_0(0, 0)|^2 = 4 \quad (17.3.14)$$

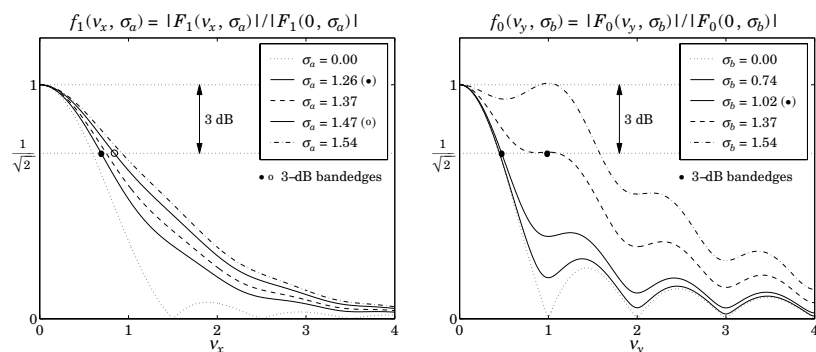
The mainlobe/sidelobe characteristics of the gain functions  $g_H(\theta)$  and  $g_E(\theta)$  depend essentially on the two functions:

$$f_1(v_x, \sigma_a) = \left| \frac{F_1(v_x, \sigma_a)}{F_1(0, \sigma_a)} \right|, \quad f_0(v_y, \sigma_b) = \left| \frac{F_0(v_y, \sigma_b)}{F_0(0, \sigma_b)} \right| \quad (17.3.15)$$

Fig. 17.3.1 shows these functions for the following values of the  $\sigma$ -parameters:  $\sigma_a = [0, 1.2593, 1.37, 1.4749, 1.54]$  and  $\sigma_b = [0, 0.7375, 1.0246, 1.37, 1.54]$ .

The values  $\sigma_a = 1.2593$  and  $\sigma_b = 1.0246$  are the optimum values that maximize the horn directivity (they are close to the commonly used values of  $\sigma_a = \sqrt{1.5} = 1.2247$  and  $\sigma_b = 1$ ).

The values  $\sigma_a = 1.4749$  and  $\sigma_b = \sigma_a/2 = 0.7375$  are the optimum values that achieve the highest directivity for a waveguide and horn that have the same aspect ratio of  $b/a = B/A = 1/2$ .

Fig. 17.3.1 Gain functions for different  $\sigma$ -parameters.

For  $\sigma_a = \sigma_b = 0$ , the functions reduce to the sinc and double-sinc functions of Eq. (17.3.6). The value  $\sigma_b = 1.37$  was chosen because the function  $f_0(v_y, \sigma_b)$  develops a plateau at the 3-dB level, making the definition of the 3-dB width ambiguous.

The value  $\sigma_b = 1.54$  was chosen because  $f_0(v_y, \sigma_b)$  exhibits a secondary maximum away from  $v_y = 0$ . This maximum becomes stronger as  $\sigma_b$  is increased further.

The functions  $f_1(v, \sigma)$  and  $f_0(v, \sigma)$  can be evaluated for any vector of  $v$ -values and any  $\sigma$  with the help of the function `diffint`. For example, the following code computes them over the interval  $0 \leq v \leq 4$  for the optimum values  $\sigma_a = 1.2593$  and  $\sigma_b = 1.0246$ , and also determines the 3-dB bandedges with the help of the function `hband`:

```
sa = 1.2593; sb = 1.0249;
v = 0:0.01:4;
```

```
f1 = abs(diffint(v,sa,1) / diffint(0,sa,1));
f0 = abs(diffint(v,sb,0) / diffint(0,sb,0));
```

```
va = hband(sa,1); % 3-dB bandedge for H-plane pattern
vb = hband(sb,0); % 3-dB bandedge for E-plane pattern
```

The mainlobes become wider as  $\sigma_a$  and  $\sigma_b$  increase. The 3-dB bandedges corresponding to the optimum  $\sigma$ s are found from `hband` to be  $v_a = 0.6928$  and  $v_b = 0.4737$ , and are shown on the graphs.

The 3-dB width in angle  $\theta$  can be determined from  $v_x = (A/\lambda) \sin \theta$ , which gives approximately  $\Delta\theta_a = (2v_a) (\lambda/A)$ —the approximation being good for  $A > 2\lambda$ . Thus, in radians and in degrees, we obtain the  $H$ -plane and  $E$ -plane optimum 3-dB widths:

$$\Delta\theta_a = 1.3856 \frac{\lambda}{A} = 79.39^\circ \frac{\lambda}{A}, \quad \Delta\theta_b = 0.9474 \frac{\lambda}{B} = 54.28^\circ \frac{\lambda}{B} \quad (17.3.16)$$

The indicated angles must be replaced by  $77.90^\circ$  and  $53.88^\circ$  if the near-optimum  $\sigma$ s are used instead, that is,  $\sigma_a = 1.2247$  and  $\sigma_b = 1$ .

Because of the 3-dB plateau of  $f_0(v_y, \sigma_b)$  at or near  $\sigma_b = 1.37$ , the function `hband` defines the bandedge to be in the middle of the plateau. At  $\sigma_b = 1.37$ , the computed bandedge is  $v_b = 0.9860$ , and is shown in Fig. 17.3.1.

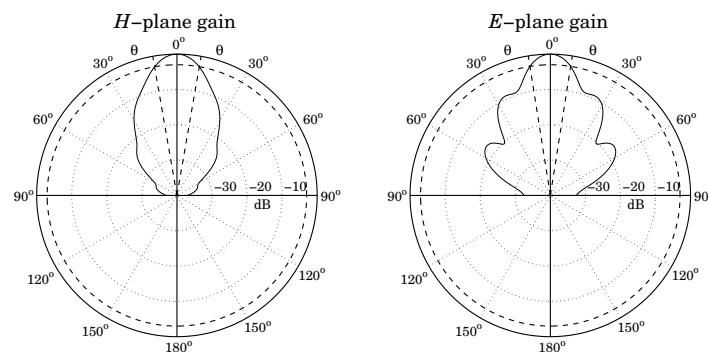
The 3-dB bandedges for the parameters  $\sigma_a = 1.4749$  and  $\sigma_b = 0.7375$  corresponding to aspect ratio of 1/2 are  $v_a = 0.8402$  (shown on the left graph) and  $v_b = 0.4499$ .

The MATLAB function `hgain` computes the gains  $g_H(\theta)$  and  $g_E(\theta)$  at  $N+1$  equally spaced angles over the interval  $[0, \pi/2]$ , given the horn dimensions  $A, B$  and the parameters  $\sigma_a, \sigma_b$ . It has usage:

```
[gh,ge,th] = hgain(N,A,B,sa,sb); % note: th = linspace(0, pi/2, N+1)
[gh,ge,th] = hgain(N,A,B); % uses optimum values sigma_a = 1.2593, sigma_b = 1.0246
```

**Example 17.3.1:** Fig. 17.3.2 shows the  $H$ - and  $E$ -plane gains of a horn with sides  $A = 4\lambda$  and  $B = 3\lambda$  and for the optimum values of the  $\sigma$ -parameters. The 3-dB angle widths were computed from Eq. (17.3.16) to be:  $\Delta\theta_a = 19.85^\circ$  and  $\Delta\theta_b = 18.09^\circ$ .

The graphs show also a 3-dB gain circle as it intersects the gain curves at the 3-dB angles, which are  $\Delta\theta_a/2$  and  $\Delta\theta_b/2$ .

Fig. 17.3.2  $H$ - and  $E$ -plane gains for  $A = 4\lambda$ ,  $B = 3\lambda$ , and  $\sigma_a = 1.2593$ ,  $\sigma_b = 1.0246$ .

The essential MATLAB code for generating the left graph was:

```
A = 4; B = 3; N = 200;
[gh,ge,th] = hgain(N,A,B); % calculate gains
Dtha = 79.39/A; % calculate width Delta theta_ba
dbp(th,gh); % make polar plot in dB
addbwp(Dtha); % add the 3-dB widths
addcirc(3); % add a 3-dB gain circle
```

We will see later that the gain of this horn is  $G = 18.68$  dB and that it can fit on a waveguide with sides  $a = \lambda$  and  $b = 0.35\lambda$ , with an axial length of  $R_A = R_B = 3.78\lambda$ . □

## 17.4 Horn Directivity

The radiated power  $P_{\text{rad}}$  is obtained by integrating the Poynting vector of the aperture fields over the horn area. The quadratic phase factors in Eq. (17.2.9) have no effect on this calculation, the result being the same as in the case of a waveguide. Thus,

$$P_{\text{rad}} = \frac{1}{4\eta} |E_0|^2 (AB) \quad (17.4.1)$$

It follows that the horn directivity will be:

$$G = 4\pi \frac{U_{\text{max}}}{P_{\text{rad}}} = \frac{4\pi}{\lambda^2} (AB) \frac{1}{8} |F_1(0, \sigma_a) F_0(0, \sigma_b)|^2 = e \frac{4\pi}{\lambda^2} AB \quad (17.4.2)$$

where we defined the aperture efficiency  $e$  by:

$$e(\sigma_a, \sigma_b) = \frac{1}{8} |F_1(0, \sigma_a) F_0(0, \sigma_b)|^2 \quad (17.4.3)$$

Using the MATLAB function `diffint`, we may compute  $e$  for any values of  $\sigma_a, \sigma_b$ . In particular, we find for the optimum values  $\sigma_a = 1.2593$  and  $\sigma_b = 1.0246$ :

$$\begin{aligned} \sigma_a = 1.2593 &\Rightarrow |F_1(0, \sigma_a)|^2 = |\text{diffint}(0, \sigma_a, 1)|^2 = 1.2520 \\ \sigma_b = 1.0246 &\Rightarrow |F_0(0, \sigma_b)|^2 = |\text{diffint}(0, \sigma_b, 0)|^2 = 3.1282 \end{aligned} \quad (17.4.4)$$

This leads to the aperture efficiency:

$$e = \frac{1}{8} (1.2520) (3.1282) \approx 0.49 \quad (17.4.5)$$

and to the optimum horn directivity:

$$G = 0.49 \frac{4\pi}{\lambda^2} AB \quad (\text{optimum horn directivity}) \quad (17.4.6)$$

If we use the near-optimum values of  $\sigma_a = \sqrt{1.5}$  and  $\sigma_b = 1$ , the calculated efficiency becomes  $e = 0.51$ . It may seem strange that the efficiency is larger for the non-optimum  $\sigma_a, \sigma_b$ . We will see in the next section that "optimum" does not mean maximizing the efficiency, but rather maximizing the gain given the geometrical constraints of the horn.

The gain-beamwidth product is from Eqs. (17.3.16) and (17.4.6),  $p = G \Delta\theta_a \Delta\theta_b = 4\pi (0.49) (1.3856) (0.9474) = 8.083 \text{ rad}^2 = 26535 \text{ deg}^2$ . Thus, in radians and in degrees, we have another instance of (14.3.14):

$$G = \frac{8.083}{\Delta\theta_a \Delta\theta_b} = \frac{26535}{\Delta\theta_a^0 \Delta\theta_b^0} \quad (17.4.7)$$

The gain of the  $H$ -plane sectoral horn is obtained by setting  $\sigma_b = 0$ , which gives  $F_0(0, 0) = 2$ . Similarly, the  $E$ -plane horn is obtained by setting  $\sigma_a = 0$ , with  $F_1(0, 0) = 4/\pi$ . Thus, we have:

$$\begin{aligned} G_H &= \frac{4\pi}{\lambda^2} (AB) \frac{1}{8} |F_1(0, \sigma_a)|^2 = \frac{2\pi}{\lambda^2} (AB) |F_1(0, \sigma_a)|^2 \\ G_E &= \frac{4\pi}{\lambda^2} (AB) \frac{16}{8\pi^2} |F_0(0, \sigma_b)|^2 = \frac{8}{\pi\lambda^2} (AB) |F_0(0, \sigma_b)|^2 \end{aligned} \quad (17.4.8)$$

The corresponding aperture efficiencies follow by dividing Eqs. (17.4.8) by  $4\pi AB/\lambda^2$ :

$$e_H(\sigma_a) = e(\sigma_a, 0) = \frac{1}{2} |F_1(0, \sigma_a)|^2, \quad e_E(\sigma_b) = e(0, \sigma_b) = \frac{2}{\pi^2} |F_0(0, \sigma_b)|^2$$

In the limit  $\sigma_a = \sigma_b = 0$ , we find  $e = 0.81$ , which agrees with Eq. (17.1.13) of the open waveguide case. The MATLAB function `heff` calculates the aperture efficiency  $e(\sigma_a, \sigma_b)$  for any values of  $\sigma_a, \sigma_b$ . It has usage:

$$e = \text{heff}(sa, sb); \quad \% \text{ horn antenna efficiency}$$

Next, we discuss the conditions for optimum directivity. In constructing a horn antenna, we have the constraints of (a) keeping the dimensions  $a, b$  of the feeding waveguide small enough so that only the  $TE_{10}$  mode is excited, and (b) maintaining the equality of the axial lengths  $R_A = R_B$  between the waveguide and horn planes, as shown in Fig. 17.2.2. Using Eqs. (17.2.1) and (17.2.8), we have:

$$R_A = \frac{A-a}{A} R_a = \frac{A(A-a)}{2\lambda\sigma_a^2}, \quad R_B = \frac{B-b}{B} R_b = \frac{B(B-b)}{2\lambda\sigma_b^2} \quad (17.4.9)$$

Then, the geometrical constraint  $R_A = R_B$  implies;

$$\frac{A(A-a)}{2\lambda\sigma_a^2} = \frac{B(B-b)}{2\lambda\sigma_b^2} \Rightarrow \frac{\sigma_b^2}{\sigma_a^2} = \frac{B(B-b)}{A(A-a)} \quad (17.4.10)$$

We wish to maximize the gain while respecting the geometry of the horn. For a fixed axial distance  $R_A = R_B$ , we wish to determine the optimum dimensions  $A, B$  that will maximize the gain.

The lengths  $R_A, R_B$  are related to the radial lengths  $R_a, R_b$  by Eq. (17.4.9). For  $A \gg a$ , the lengths  $R_a$  and  $R_A$  are practically equal, and similarly for  $R_b$  and  $R_B$ . Therefore, an almost equivalent (but more convenient) problem is to find  $A, B$  that maximize the gain for fixed values of the radial distances  $R_a, R_b$ .

Because of the relationships  $A = \sigma_a \sqrt{2\lambda R_a}$  and  $B = \sigma_b \sqrt{2\lambda R_b}$ , this problem is equivalent to finding the optimum values of  $\sigma_a$  and  $\sigma_b$  that will maximize the gain. Replacing  $A, B$  in Eq. (17.4.2), we rewrite  $G$  in the form:

$$\begin{aligned} G &= \frac{4\pi}{\lambda^2} \left( \sigma_a \sqrt{2\lambda R_a} \right) \left( \sigma_b \sqrt{2\lambda R_b} \right) \frac{1}{8} |F_1(0, \sigma_a) F_0(0, \sigma_b)|^2, \quad \text{or,} \\ G &= \frac{\pi \sqrt{R_a R_b}}{\lambda} f_a(\sigma_a) f_b(\sigma_b) \end{aligned} \quad (17.4.11)$$

where we defined the directivity functions:

$$f_a(\sigma_a) = \sigma_a |F_1(0, \sigma_a)|^2, \quad f_b(\sigma_b) = \sigma_b |F_0(0, \sigma_b)|^2 \quad (17.4.12)$$

These functions are plotted on the left graph of Fig. 17.4.1. Their maxima occur at  $\sigma_a = 1.2593$  and  $\sigma_b = 1.0246$ . As we mentioned before, these values are sometimes approximated by  $\sigma_a = \sqrt{1.5} = 1.2244$  and  $\sigma_b = 1$ .

An alternative class of directivity functions can be derived by constructing a horn whose aperture has the *same* aspect ratio as the waveguide, that is,

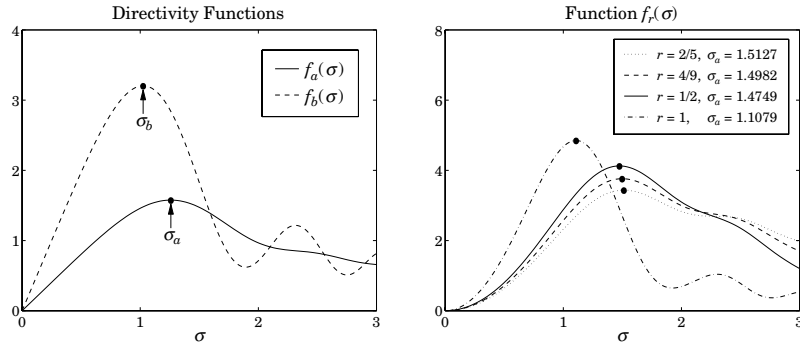


Fig. 17.4.1 Directivity functions.

$$\frac{B}{A} = \frac{b}{a} = r \tag{17.4.13}$$

The aspect ratio of a typical waveguide is of the order of  $r = 0.5$ , which ensures the largest operating bandwidth in the  $TE_{10}$  mode and the largest power transmitted.

It follows from Eq. (17.4.13) that (17.4.10) will be satisfied provided  $\sigma_b^2/\sigma_a^2 = r^2$ , or  $\sigma_b = r\sigma_a$ . The directivity (17.4.11) becomes:

$$G = \frac{\pi\sqrt{R_a R_b}}{\lambda} f_r(\sigma_a) \tag{17.4.14}$$

where we defined the function:

$$f_r(\sigma_a) = f_a(\sigma_a)f_b(r\sigma_a) = r\sigma_a^2 |F_1(0, \sigma_a)F_0(0, r\sigma_a)|^2 \tag{17.4.15}$$

This function has a maximum, which depends on the aspect ratio  $r$ . The right graph of Fig. 17.4.1 shows  $f_r(\sigma)$  and its maxima for various values of  $r$ . The aspect ratio  $r = 1/2$  is used in many standard guides,  $r = 4/9$  is used in the WR-90 waveguide, and  $r = 2/5$  in the WR-42.

The MATLAB function `hsigma` computes the optimum  $\sigma_a$  and  $\sigma_b = r\sigma_a$  for a given aspect ratio  $r$ . It has usage:

```
[sa, sb] = hsigma(r); % optimum σ-parameters
```

With input  $r = 0$ , it outputs the separate optimal values  $\sigma_a = 1.2593$  and  $\sigma_b = 1.0246$ . For  $r = 0.5$ , it gives  $\sigma_a = 1.4749$  and  $\sigma_b = \sigma_a/2 = 0.7375$ , with corresponding aperture efficiency  $e = 0.4743$ .

### 17.5 Horn Design

The design problem for a horn antenna is to determine the sides  $A, B$  that will achieve a given gain  $G$  and will also fit geometrically with a given waveguide of sides  $a, b$ , satisfying

the condition  $R_A = R_B$ . The two design equations for  $A, B$  are then Eqs. (17.4.2) and (17.4.10):

$$G = e \frac{4\pi}{\lambda^2} AB, \quad \frac{\sigma_b^2}{\sigma_a^2} = \frac{B(B-b)}{A(A-a)} \tag{17.5.1}$$

The design of the constant aspect ratio case is straightforward. Because  $\sigma_b = r\sigma_a$ , the second condition is already satisfied. Then, the first condition can be solved for  $A$ , from which one obtains  $B = rA$  and  $R_A = A(A-a)/(2\lambda\sigma_a^2)$ :

$$G = e \frac{4\pi}{\lambda^2} A(rA) \Rightarrow A = \lambda \sqrt{\frac{G}{4\pi e r}} \tag{17.5.2}$$

In Eq. (17.5.2), the aperture efficiency  $e$  must be calculated from Eq. (17.4.3) with the help of the MATLAB function `heff`.

For unequal aspect ratios and arbitrary  $\sigma_a, \sigma_b$ , one must solve the system of equations (17.5.1) for the two unknowns  $A, B$ . To avoid negative solutions for  $B$ , the second equation in (17.5.1) can be solved for  $B$  in terms of  $A, a, b$ , thus replacing the above system with:

$$f_1(A, B) \equiv B - \left[ \frac{b}{2} + \sqrt{\frac{b^2}{4} + \frac{\sigma_b^2}{\sigma_a^2} A(A-a)} \right] = 0 \tag{17.5.3}$$

$$f_2(A, B) \equiv AB - \frac{\lambda^2 G}{4\pi e} = 0$$

This system can be solved iteratively using Newton's method, which amounts to starting with some initial values  $A, B$  and keep replacing them with the corrected values  $A + \Delta A$  and  $B + \Delta B$ , where the corrections are computed from:

$$\begin{bmatrix} \Delta A \\ \Delta B \end{bmatrix} = -\mathcal{M}^{-1} \begin{bmatrix} f_1 \\ f_2 \end{bmatrix}, \quad \text{where } \mathcal{M} = \begin{bmatrix} \partial_A f_1 & \partial_B f_1 \\ \partial_A f_2 & \partial_B f_2 \end{bmatrix}$$

The matrix  $\mathcal{M}$  is given by:

$$\mathcal{M} = \begin{bmatrix} -\frac{\sigma_b^2}{\sigma_a^2} & \frac{2A-a}{(2B-b-2f_1)} & 1 \\ -\frac{\sigma_b^2}{\sigma_a^2} & \frac{2A-a}{B} & 1 \end{bmatrix} \approx \begin{bmatrix} -\frac{\sigma_b^2}{\sigma_a^2} & \frac{2A-a}{B} & 1 \\ -\frac{\sigma_b^2}{\sigma_a^2} & \frac{2B-b}{B} & 1 \end{bmatrix}$$

where we replaced the  $2f_1$  term by zero (this is approximately correct near convergence). Good initial values are obtained by assuming that  $A, B$  will be much larger than  $a, b$  and therefore, we write Eq. (17.5.1) approximately in the form:

$$G = e \frac{4\pi}{\lambda^2} AB, \quad \frac{\sigma_b^2}{\sigma_a^2} = \frac{B^2}{A^2} \tag{17.5.4}$$

This system can be solved easily, giving the initial values:

$$A_0 = \lambda \sqrt{\frac{G}{4\pi e} \frac{\sigma_a}{\sigma_b}}, \quad B_0 = \lambda \sqrt{\frac{G}{4\pi e} \frac{\sigma_b}{\sigma_a}} \tag{17.5.5}$$

Note that these are the same solutions as in the constant- $r$  case. The algorithm converges extremely fast, requiring about 3-5 iterations. It has been implemented by the MATLAB function `hopt` with usage:



```
[A,B,R,err] = hopt(G,a,b,sa,sb); % optimum horn antenna design
[A,B,R,err] = hopt(G,a,b,sa,sb,N); % N is the maximum number of iterations
[A,B,R,err] = hopt(G,a,b,sa,sb,0); % outputs initial values only
```

where  $G$  is the desired gain in dB,  $a, b$  are the waveguide dimensions. The output  $R$  is the common axial length  $R = R_A = R_B$ . All lengths are given in units of  $\lambda$ . If the parameters  $\sigma_a, \sigma_b$  are omitted, their optimum values are used. The quantity  $err$  is the approximation error, and  $N$ , the maximum number of iterations (default is 10).

**Example 17.5.1:** Design a horn antenna with gain 18.68 dB and waveguide sides of  $a = \lambda$  and  $b = 0.35\lambda$ . The following call to `hopt`,

```
[A,B,R,err] = hopt(18.68, 1, 0.35);
```

yields the values (in units of  $\lambda$ ):  $A = 4$ ,  $B = 2.9987$ ,  $R = 3.7834$ , and  $err = 3.7 \times 10^{-11}$ . These are the same as in Example 17.3.1.  $\square$

**Example 17.5.2:** Design a horn antenna operating at 10 GHz and fed by a WR-90 waveguide with sides  $a = 2.286$  cm and  $b = 1.016$  cm. The required gain is 23 dB ( $G = 200$ ).

**Solution:** The wavelength is  $\lambda = 3$  cm. We carry out two designs, the first one using the optimum values  $\sigma_a = 1.2593$ ,  $\sigma_b = 1.0246$ , and the second using the aspect ratio of the WR-90 waveguide, which is  $r = b/a = 4/9$ , and corresponds to  $\sigma_a = 1.4982$  and  $\sigma_b = 0.6659$ . The following MATLAB code calculates the horn sides for the two designs and plots the  $E$ -plane patterns:

```
l_a = 3; a = 2.286; b = 1.016; % lengths in cm
G = 200; Gdb = 10*log10(G); % Gdb = 23.0103 dB

[sa1,sb1] = hsigma(0); % optimum sigma-parameters
[A1,B1,R1] = hopt(Gdb, a/l_a, b/l_a, sa1, sb1); % Ab1, Bb1, Rb1 in units of lambda

[sa2,sb2] = hsigma(b/a); % optimum sigma's for r = b/a
[A2,B2,R2] = hopt(Gdb, a/l_a, b/l_a, sa2, sb2, 0); % output initial values

N = 200; % 201 angles in 0 <= theta <= pi/2

[gh1,ge1,th] = hgain(N,A1,B1,sa1,sb1); % calculate gains
[gh2,ge2,th] = hgain(N,A2,B2,sa2,sb2);

figure; dbp(th,gh1); figure; dbp(th,ge1); % polar plots in dB
figure; dbp(th,gh2); figure; dbp(th,ge2);

A1 = A1*l_a; B1 = B1*l_a; R1 = R1*l_a; % lengths in cm
A2 = A2*l_a; B2 = B2*l_a; R2 = R2*l_a;
```

The designed sides and axial lengths are in the two cases:

$$\begin{aligned} A_1 &= 19.2383 \text{ cm}, & B_1 &= 15.2093 \text{ cm}, & R_1 &= 34.2740 \text{ cm} \\ A_2 &= 26.1457 \text{ cm}, & B_2 &= 11.6203 \text{ cm}, & R_2 &= 46.3215 \text{ cm} \end{aligned}$$

The  $H$ - and  $E$ -plane patterns are plotted in Fig. 17.5.1. The first design (top graphs) has slightly wider 3-dB width in the  $H$ -plane because its  $A$ -side is shorter than that of the second design. But, its  $E$ -plane 3-dB width is narrower because its  $B$ -side is longer.

The initial values given in Eq. (17.5.5) can be used to give an alternative, albeit approximate, solution obtained purely algebraically: Compute  $A_0, B_0$ , then revise the value of  $B_0$  by recomputing it from the first of Eq. (17.5.3), so that the geometric constraint  $R_A = R_B$  is met, and then recompute the gain, which will be slightly different than the required one.

For example, using the optimum values  $\sigma_a = 1.2593$  and  $\sigma_b = 1.0246$ , we find from (17.5.5):  $A_0 = 18.9644$ ,  $B_0 = 15.4289$  cm, and  $R_A = 33.2401$  cm. Then, we recalculate  $B_0$  to be  $B_0 = 13.9453$  cm, and obtain the new gain  $G = 180.77$ , or, 22.57 dB.  $\square$

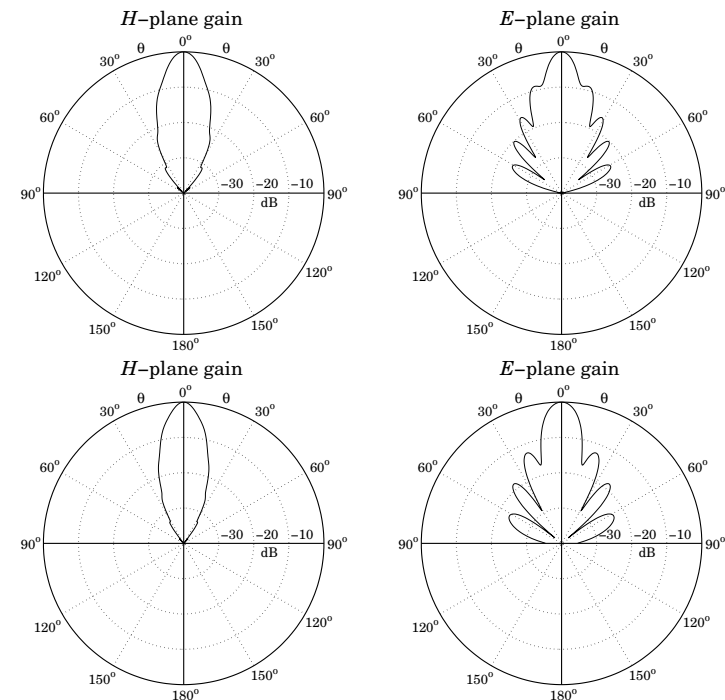


Fig. 17.5.1  $H$ - and  $E$ -plane patterns.

## 17.6 Microstrip Antennas

A microstrip antenna is a metallic patch on top of a dielectric substrate that sits on top of a ground plane. Fig. 17.6.1 depicts a rectangular microstrip antenna fed by a microstrip line. It can also be fed by a coaxial line, with its inner and outer conductors connected to the patch and ground plane, respectively.

In this section, we consider only rectangular patches and discuss simple aperture models for calculating the radiation patterns of the antenna. Further details and applications of microstrip antennas may be found in [765-772].

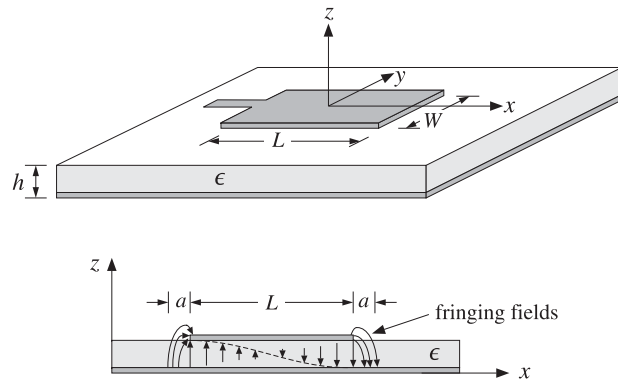


Fig. 17.6.1 Microstrip antenna and  $E$ -field pattern in substrate.

The height  $h$  of the substrate is typically of a fraction of a wavelength, such as  $h = 0.05\lambda$ , and the length  $L$  is of the order of  $0.5\lambda$ . The structure radiates from the fringing fields that are exposed above the substrate at the edges of the patch.

In the so-called cavity model, the patch acts as resonant cavity with an electric field perpendicular to the patch, that is, along the  $z$ -direction. The magnetic field has vanishing tangential components at the four edges of the patch. The fields of the lowest resonant mode (assuming  $L \geq W$ ) are given by:

$$\begin{aligned} E_z(x) &= -E_0 \sin\left(\frac{\pi x}{L}\right) & -\frac{L}{2} \leq x \leq \frac{L}{2} \\ H_y(x) &= -H_0 \cos\left(\frac{\pi x}{L}\right) & -\frac{W}{2} \leq y \leq \frac{W}{2} \end{aligned} \quad \text{for} \quad (17.6.1)$$

where  $H_0 = -jE_0/\eta$ . We have placed the origin at the middle of the patch (note that  $E_z(x)$  is equivalent to  $E_0 \cos(\pi x/L)$  for  $0 \leq x \leq L$ .)

It can be verified that Eqs. (17.6.1) satisfy Maxwell's equations and the boundary conditions, that is,  $H_y(x) = 0$  at  $x = \pm L/2$ , provided the resonant frequency is:

$$\omega = \frac{\pi c}{L} \Rightarrow f = 0.5 \frac{c}{L} = 0.5 \frac{c_0}{L\sqrt{\epsilon_r}} \quad (17.6.2)$$

where  $c = c_0/\sqrt{\epsilon_r}$ ,  $\eta = \eta_0/\sqrt{\epsilon_r}$ , and  $\epsilon_r$  is the relative permittivity of the dielectric substrate. It follows that the resonant microstrip length will be half-wavelength:

$$L = 0.5 \frac{\lambda}{\sqrt{\epsilon_r}} \quad (17.6.3)$$

Fig. 17.6.2 shows two simple models for calculating the radiation patterns of the microstrip antenna. The model on the left assumes that the fringing fields extend over a small distance  $a$  around the patch sides and can be replaced with the fields  $E_a$  that are tangential to the *substrate surface* [767]. The four extended edge areas around the patch serve as the effective radiating apertures.

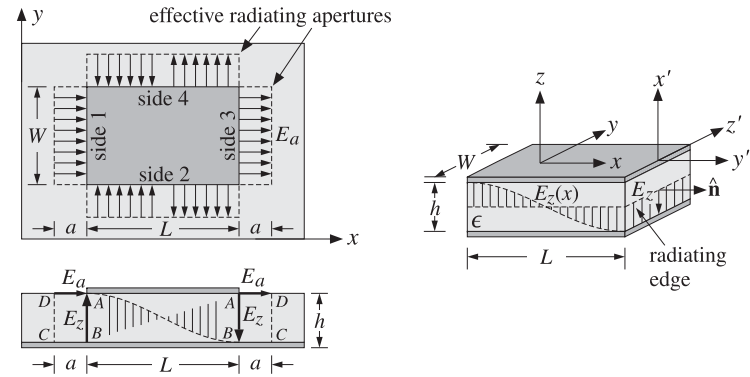


Fig. 17.6.2 Aperture models for microstrip antenna.

The model on the right assumes that the substrate is truncated beyond the extent of the patch [766]. The four dielectric substrate walls serve now as the radiating apertures. The only tangential aperture field on these walls is  $E_a = \hat{z}E_z$ , because the tangential magnetic fields vanish by the boundary conditions.

For both models, the ground plane can be eliminated using image theory, resulting in doubling the aperture magnetic currents, that is,  $J_{ms} = -2\hat{n} \times E_a$ . The radiation patterns are then determined from  $J_{ms}$ .

For the first model, the effective tangential fields can be expressed in terms of the field  $E_z$  by the relationship:  $aE_a = hE_z$ . This follows by requiring the vanishing of the line integrals of  $E$  around the loops labeled ABCD in the lower left of Fig. 17.6.2. Because  $E_z = \pm E_0$  at  $x = \pm L/2$ , we obtain from the left and right such contours:

$$\oint_{ABCD} E \cdot d\mathbf{l} = -E_0 h + E_a a = 0, \quad \oint_{ABCD} E \cdot d\mathbf{l} = E_0 h - E_a a = 0 \Rightarrow E_a = \frac{hE_0}{a}$$

In obtaining these, we assumed that the electric field is nonzero only along the sides AD and AB. A similar argument for the sides 2 & 4 shows that  $E_a = \pm hE_z(x)/a$ . The directions of  $E_a$  at the four sides are as shown in the figure. Thus, we have:

$$\begin{aligned} \text{for sides 1 \& 3:} \quad E_a &= \hat{x} \frac{hE_0}{a} \\ \text{for sides 2 \& 4:} \quad E_a &= \pm \hat{y} \frac{hE_z(x)}{a} = \mp \hat{y} \frac{hE_0}{a} \sin\left(\frac{\pi x}{L}\right) \end{aligned} \quad (17.6.4)$$

The outward normal to the aperture plane is  $\hat{n} = \hat{z}$  for all four sides. Therefore, the surface magnetic currents  $J_{ms} = -2\hat{n} \times E_a$  become:

$$\begin{aligned} \text{for sides 1 \& 3:} \quad J_{ms} &= \hat{y} \frac{2hE_0}{a} \\ \text{for sides 2 \& 4:} \quad J_{ms} &= \pm \hat{x} \frac{2hE_0}{a} \sin\left(\frac{\pi x}{L}\right) \end{aligned} \quad (17.6.5)$$

The radiated electric field is obtained from Eq. (16.3.4) by setting  $F = 0$  and calculating  $F_m$  as the sum of the magnetic radiation vectors over the four effective apertures:

$$\mathbf{E} = jk \frac{e^{-jkr}}{4\pi r} \hat{\mathbf{r}} \times \mathbf{F}_m = jk \frac{e^{-jkr}}{4\pi r} \hat{\mathbf{r}} \times [\mathbf{F}_{m1} + \mathbf{F}_{m2} + \mathbf{F}_{m3} + \mathbf{F}_{m4}] \quad (17.6.6)$$

The vectors  $\mathbf{F}_m$  are the two-dimensional Fourier transforms over the apertures:

$$\mathbf{F}_m(\theta, \phi) = \int_A \mathbf{J}_{ms}(x, y) e^{jk_x x + jk_y y} dS$$

The integration surfaces  $dS = dx dy$  are approximately,  $dS = ady$  for 1 & 3, and  $dS = adx$  for 2 & 4. Similarly, in the phase factor  $e^{jk_x x + jk_y y}$ , we must set  $x = \mp L/2$  for sides 1 & 3, and  $y = \mp W/2$  for sides 2 & 4. Inserting Eq. (17.6.5) into the Fourier integrals and combining the terms for apertures 1 & 3 and 2 & 4, we obtain:

$$\begin{aligned} \mathbf{F}_{m,13} &= \hat{\mathbf{y}} \frac{2hE_0}{a} \int_{-W/2}^{W/2} (e^{-jk_x L/2} + e^{jk_x L/2}) e^{jk_y y} a dy \\ \mathbf{F}_{m,24} &= \hat{\mathbf{x}} \frac{2hE_0}{a} \int_{-L/2}^{L/2} (e^{-jk_y W/2} - e^{jk_y W/2}) \sin\left(\frac{\pi x}{L}\right) e^{jk_x x} a dx \end{aligned}$$

Note that the  $a$  factors cancel. Using Euler's formulas and the integrals:

$$\int_{-W/2}^{W/2} e^{jk_y y} dy = W \frac{\sin(k_y W/2)}{k_y W/2}, \quad \int_{-L/2}^{L/2} \sin\left(\frac{\pi x}{L}\right) e^{jk_x x} dx = \frac{2jk_x L^2}{\pi^2} \frac{\cos(k_x L/2)}{1 - \left(\frac{k_x L}{\pi}\right)^2},$$

we find the radiation vectors:

$$\begin{aligned} \mathbf{F}_{m,12} &= \hat{\mathbf{y}} 4E_0 h W \cos(\pi v_x) \frac{\sin(\pi v_y)}{\pi v_y} \\ \mathbf{F}_{m,24} &= \hat{\mathbf{x}} 4E_0 h L \frac{4v_x \cos(\pi v_x)}{\pi(1 - 4v_x^2)} \sin(\pi v_y) \end{aligned} \quad (17.6.7)$$

where we defined the normalized wavenumbers as usual:

$$\begin{aligned} v_x &= \frac{k_x L}{2\pi} = \frac{L}{\lambda} \sin \theta \cos \phi \\ v_y &= \frac{k_y W}{2\pi} = \frac{W}{\lambda} \sin \theta \sin \phi \end{aligned} \quad (17.6.8)$$

From Eq. (E.8) of Appendix E, we have:

$$\begin{aligned} \hat{\mathbf{r}} \times \hat{\mathbf{y}} &= \hat{\mathbf{r}} \times (\hat{\mathbf{r}} \sin \theta \sin \phi + \hat{\boldsymbol{\theta}} \cos \theta \sin \phi + \hat{\boldsymbol{\phi}} \cos \phi) = \hat{\boldsymbol{\phi}} \cos \theta \sin \phi - \hat{\boldsymbol{\theta}} \cos \phi \\ \hat{\mathbf{r}} \times \hat{\mathbf{x}} &= \hat{\mathbf{r}} \times (\hat{\mathbf{r}} \sin \theta \cos \phi + \hat{\boldsymbol{\theta}} \cos \theta \cos \phi - \hat{\boldsymbol{\phi}} \sin \phi) = \hat{\boldsymbol{\phi}} \cos \theta \cos \phi + \hat{\boldsymbol{\theta}} \sin \phi \end{aligned}$$

It follows from Eq. (17.6.6) that the radiated fields from sides 1 & 3 will be:

$$\mathbf{E}(\theta, \phi) = jk \frac{e^{-jkr}}{4\pi r} 4E_0 h W [\hat{\boldsymbol{\phi}} \cos \theta \sin \phi - \hat{\boldsymbol{\theta}} \cos \phi] F(\theta, \phi) \quad (17.6.9)$$

where we defined the function:

$$F(\theta, \phi) = \cos(\pi v_x) \frac{\sin(\pi v_y)}{\pi v_y} \quad (17.6.10)$$

Similarly, we have for sides 2 & 4:

$$\begin{aligned} \mathbf{E}(\theta, \phi) &= jk \frac{e^{-jkr}}{4\pi r} 4E_0 h L [\hat{\boldsymbol{\phi}} \cos \theta \cos \phi + \hat{\boldsymbol{\theta}} \sin \phi] f(\theta, \phi) \\ f(\theta, \phi) &= \frac{4v_x \cos(\pi v_x)}{\pi(1 - 4v_x^2)} \sin(\pi v_y) \end{aligned} \quad (17.6.11)$$

The normalized gain is found from Eq. (17.6.9) to be:

$$g(\theta, \phi) = \frac{|\mathbf{E}(\theta, \phi)|^2}{|E|_{\max}^2} = (\cos^2 \theta \sin^2 \phi + \cos^2 \phi) |F(\theta, \phi)|^2 \quad (17.6.12)$$

The corresponding expression for sides 2 & 4, although not normalized, provides a measure for the gain in that case:

$$g(\theta, \phi) = (\cos^2 \theta \cos^2 \phi + \sin^2 \phi) |f(\theta, \phi)|^2 \quad (17.6.13)$$

The  $E$ - and  $H$ -plane gains are obtained by setting  $\phi = 0^\circ$  and  $\phi = 90^\circ$  in Eq. (17.6.12):

$$\begin{aligned} g_E(\theta) &= \frac{|E_\theta|^2}{|E_\theta|_{\max}^2} = |\cos(\pi v_x)|^2, & v_x &= \frac{L}{\lambda} \sin \theta \\ g_H(\theta) &= \frac{|E_\phi|^2}{|E_\phi|_{\max}^2} = \left| \cos \theta \frac{\sin(\pi v_y)}{\pi v_y} \right|^2, & v_y &= \frac{W}{\lambda} \sin \theta \end{aligned} \quad (17.6.14)$$

Most of the radiation from the microstrip arises from sides 1 & 3. Indeed,  $F(\theta, \phi)$  has a maximum towards broadside,  $v_x = v_y = 0$ , whereas  $f(\theta, \phi)$  vanishes. Moreover,  $f(\theta, \phi)$  vanishes identically for all  $\theta$  and  $\phi = 0^\circ$  ( $E$ -plane) or  $\phi = 90^\circ$  ( $H$ -plane).

Therefore, sides 2 & 4 contribute little to the total radiation, and they are usually ignored. For lengths of the order of  $L = 0.3\lambda$  to  $L = \lambda$ , the gain function (17.6.13) remains suppressed by 7 to 17 dB for *all directions*, relative to the gain of (17.6.12).

**Example 17.6.1:** Fig. 17.6.3 shows the  $E$ - and  $H$ -plane patterns for  $W = L = 0.3371\lambda$ . Both patterns are fairly broad.

The choice for  $L$  comes from the resonant condition  $L = 0.5\lambda/\sqrt{\epsilon_r}$ . For a typical substrate with  $\epsilon_r = 2.2$ , we find  $L = 0.5\lambda/\sqrt{2.2} = 0.3371\lambda$ .

Fig. 17.6.4 shows the 3-dimensional gains computed from Eqs. (17.6.12) and (17.6.13). The field strengths (square roots of the gains) are plotted to improve the visibility of the graphs. The MATLAB code for generating these plots was:

```
L = 0.5/sqrt(2.2); W = L;
[th,ph] = meshgrid(0:3:90, 0:6:360); th = th * pi/180; ph = ph * pi/180;
vx = L * sin(th) .* cos(ph);
vy = W * sin(th) .* sin(ph);
```

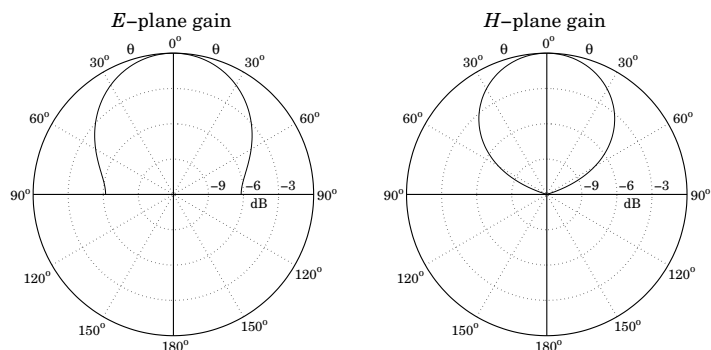


Fig. 17.6.3 E- and H-plane gains of microstrip antenna.

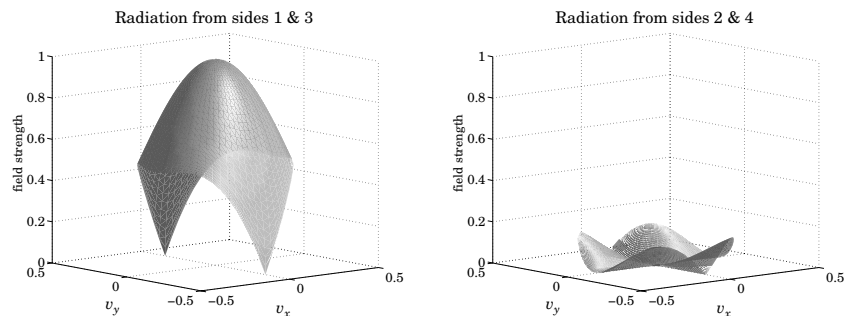


Fig. 17.6.4 Two-dimensional gain patterns from sides 1 & 3 and 2 & 4.

```

E13 = sqrt(cos(th).^2.*sin(ph).^2 + cos(ph).^2);
E13 = E13 .* abs(cos(pi*vx) .* sinc(vy));

figure; surf1(vx,vy,E13);
shading interp; colormap(gray(32));

view([-40,10]);

E24 = sqrt(cos(th).^2.*cos(ph).^2 + sin(ph).^2);
E24 = E24 .* abs(4*vx.*dsinc(vx)/pi .* sin(pi*vy));

figure; surf1(vx,vy,E24);
shading interp; colormap(gray(32));
    
```

The gain from sides 2 & 4 vanishes along the  $v_x$ - and  $v_y$  axes, while its maximum in all directions is  $\sqrt{g} = 0.15$  or  $-16.5$  dB. □

Using the alternative aperture model shown on the right of Fig. 17.6.2, one obtains identical expressions for the magnetic current densities  $J_{ms}$  along the four sides, and

therefore, identical radiation patterns. The integration surfaces are now  $dS = hdy$  for sides 1 & 3, and  $dS = hdx$  for 2 & 4.

### 17.7 Parabolic Reflector Antennas

Reflector antennas are characterized by very high gains (30 dB and higher) and narrow main beams. They are widely used in satellite and line-of-sight microwave communications and in radar.

At microwave frequencies, the most common feeds are rectangular, circular, or corrugated horns. Dipole feeds—usually backed by a reflecting plane to enhance their radiation towards the reflector—are used at lower frequencies, typically, up to UHF. Some references on reflector antennas and feed design are [745–764].

A typical parabolic reflector, fed by a horn antenna positioned at the focus of the parabola, is shown in Fig. 17.7.1. A geometrical property of parabolas is that all rays originating from the focus get reflected in a direction parallel to the parabola’s axis, that is, the  $z$  direction.

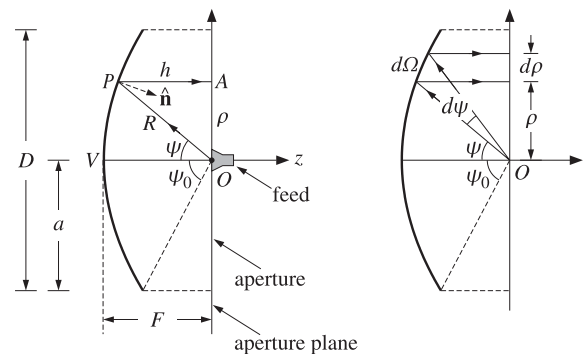


Fig. 17.7.1 Parabolic reflector antenna with feed at the focus.

We choose the origin to be at the focus. An incident ray  $OP$  radiated from the feed at an angle  $\psi$  becomes the reflected ray  $PA$  parallel to the  $z$ -axis. The projection of all the reflected rays onto a plane perpendicular to the  $z$ -axis—such as the  $xy$ -plane—can be considered to be the effective *aperture* of the antenna. This is shown in Fig. 17.7.2.

Let  $R$  and  $h$  be the lengths of the rays  $OP$  and  $PA$ . The sum  $R + h$  represents the total optical path length from the focus to the aperture plane. This length is constant, independent of  $\psi$ , and is given by

$$R + h = 2F \tag{17.7.1}$$

where  $F$  is the focal length. The length  $2F$  is the total optical length of the incident and reflected axial rays going from  $O$  to the vertex  $V$  and back to  $O$ .

Therefore, all the rays suffer the same phase delay traveling from the focus to the plane. The spherical wave radiated from the feed gets converted upon reflection into a

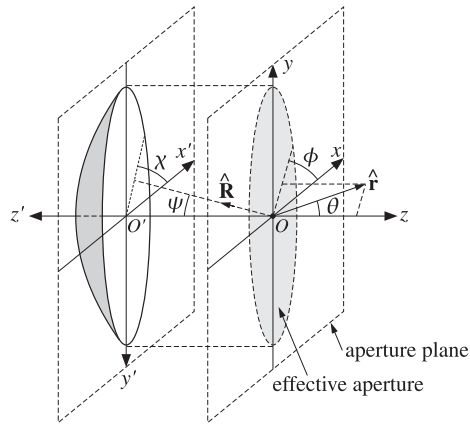


Fig. 17.7.2 Parabolic antenna and its projected effective aperture.

plane wave. Conversely, for a receiving antenna, an incident plane wave gets converted into a spherical wave converging onto the focus.

Since  $h = R \cos \psi$ , Eq. (17.7.1) can be written in the following form, which is the polar representation of the parabolic surface:

$$R + R \cos \psi = 2F \Rightarrow R = \frac{2F}{1 + \cos \psi}, \quad \text{or,} \quad (17.7.2)$$

$$\boxed{R = \frac{2F}{1 + \cos \psi} = \frac{F}{\cos^2(\psi/2)}} \quad (17.7.3)$$

The radial displacement  $\rho$  of the reflected ray on the aperture plane is given by  $\rho = R \sin \psi$ . Replacing  $R$  from (17.7.3), we find:

$$\rho = 2F \frac{\sin \psi}{1 + \cos \psi} = 2F \tan \left( \frac{\psi}{2} \right) \quad (17.7.4)$$

Similarly, using  $R + h = 2F$  or  $F - h = R - F$ , we have:

$$F - h = F \frac{1 - \cos \psi}{1 + \cos \psi} = F \tan^2 \left( \frac{\psi}{2} \right) \quad (17.7.5)$$

It follows that  $h$  and  $\rho$  will be related by the equation for a parabola:

$$4F(F - h) = \rho^2 \quad (17.7.6)$$

In terms of the  $xyz$ -coordinate system, we have  $\rho^2 = x^2 + y^2$  and  $z = -h$ , so that Eq. (17.7.6) becomes the equation for a paraboloid surface:

$$\boxed{4F(F + z) = x^2 + y^2} \quad (17.7.7)$$

The diameter  $D$ , or the radius  $a = D/2$ , of the reflector and its focal length  $F$  determine the maximum angle  $\psi$ . It is obtained by setting  $\rho = a$  in Eq. (17.7.4):

$$a = \frac{D}{2} = 2F \tan \left( \frac{\psi_0}{2} \right) \Rightarrow \boxed{\psi_0 = 2 \operatorname{atan} \left( \frac{D}{4F} \right)} \quad (17.7.8)$$

Thus, the  $F/D$  ratio determines  $\psi_0$ . For example, if  $F/D = 0.25, 0.35, 0.50$ , then  $\psi_0 = 90^\circ, 71^\circ, 53^\circ$ . Practical  $F/D$  ratios are in the range 0.25–0.50.

### 17.8 Gain and Beamwidth of Reflector Antennas

To determine the radiation pattern of a reflector antenna, one may use Eq. (16.4.2), provided one knows the aperture fields  $E_a, H_a$  on the effective aperture projected on the aperture plane. This approach is referred to as the *aperture-field method* [21].

Alternatively, the *current-distribution method* determines the current  $J_s$  on the surface of the reflector induced by the incident field from the feed, and then applies Eq. (16.4.1) with  $J_{ms} = 0$ , using the curved surface of the reflector as the integration surface ( $J_{ms}$  vanishes on the reflector surface because there are no tangential electric fields on a perfect conductor.)

The two methods yield slightly different, but qualitatively similar, results for the radiation patterns. The aperture fields  $E_a, H_a$  and the surface current  $J_s$  are determined by geometrical optics considerations based on the assumptions that (a) the reflector lies in the radiation zone of the feed antenna, and (b) the incident field from the feed gets reflected as if the reflector surface is perfectly conducting and locally flat. These assumptions are justified because in practice the size of the reflector and its curvature are much larger than the wavelength  $\lambda$ .

We use the polar and azimuthal angles  $\psi$  and  $\chi$  indicated on Fig. 17.7.2 to characterize the direction  $\hat{\mathbf{R}}$  of an incident ray from the feed to the reflector surface.

The radiated power from the feed within the solid angle  $d\Omega = \sin \psi d\psi d\chi$  must be equal upon reflection to the power propagating parallel to the  $z$ -axis and intercepting the aperture plane through the area  $dA = \rho d\rho d\chi$ , as depicted in Fig. 17.7.1.

Assuming that  $U_{\text{feed}}(\psi, \chi)$  is the feed antenna's *radiation intensity* and noting that  $|E_a|^2/2\eta$  is the power density of the aperture field, the power condition reads:

$$\frac{1}{2\eta} |E_a|^2 dA = U_{\text{feed}}(\psi, \chi) d\Omega \Rightarrow \frac{1}{2\eta} |E_a|^2 \rho d\rho = U_{\text{feed}}(\psi, \chi) \sin \psi d\psi \quad (17.8.1)$$

where we divided both sides by  $d\chi$ . Differentiating Eq. (17.7.4), we have:

$$d\rho = 2F \frac{d\psi}{2} \frac{1}{\cos^2(\psi/2)} = R d\psi$$

which implies that  $\rho d\rho = R^2 \sin \psi d\psi$ . Thus, solving Eq. (17.8.1) for  $|E_a|$ , we find:

$$\boxed{|E_a(\rho, \chi)| = \frac{1}{R} \sqrt{2\eta U_{\text{feed}}(\psi, \chi)}} \quad (17.8.2)$$

where we think of  $E_a$  as a function of  $\rho = 2F \tan(\psi/2)$  and  $\chi$ . Expressing  $R$  in terms of  $\rho$ , we have  $R = 2F - h = F + (F - h) = F + \rho^2/4F$ . Therefore, we may also write:

$$|E_a(\rho, \chi)| = \frac{4F}{\rho^2 + 4F^2} \sqrt{2\eta U_{\text{feed}}(\psi, \chi)} \quad (17.8.3)$$

Thus, the aperture fields get weaker towards the edge of the reflector. A measure of this tapering effect is the *edge illumination*, that is, the ratio of the electric field at the edge ( $\rho = a$ ) and at the center ( $\rho = 0$ ). Using Eqs. (17.7.3) and (17.8.2), we find:

$$\frac{|E_a(a, \chi)|}{|E_a(0, \chi)|} = \frac{1 + \cos \psi_0}{2} \sqrt{\frac{U_{\text{feed}}(\psi_0, \chi)}{U_{\text{feed}}(0, \chi)}} \quad (\text{edge illumination}) \quad (17.8.4)$$

In Sec. 16.6, we defined the directivity or gain of an aperture by Eq. (16.6.10), which we rewrite in the following form:

$$G_a = \frac{4\pi U_{\text{max}}}{P_a} \quad (17.8.5)$$

where  $P_a$  is the total power through the aperture given in terms of  $E_a$  as follows:

$$P_a = \frac{1}{2\eta} \int_A |E_a|^2 dA = \int_0^{\psi_0} \int_0^{2\pi} U_{\text{feed}}(\psi, \chi) \sin \psi d\psi d\chi \quad (17.8.6)$$

and we used Eq. (17.8.1). For a reflector antenna, the gain must be defined relative to the total power  $P_{\text{feed}}$  of the feed antenna, that is,

$$G_{\text{ant}} = \frac{4\pi U_{\text{max}}}{P_{\text{feed}}} = \frac{4\pi U_{\text{max}}}{P_a} \frac{P_a}{P_{\text{feed}}} = G_a e_{\text{spl}} \quad (17.8.7)$$

The factor  $e_{\text{spl}} = P_a/P_{\text{feed}}$  is referred to as the *spillover efficiency* or *loss* and represents the fraction of the power  $P_{\text{feed}}$  that actually gets reflected by the reflector antenna. The remaining power from the feed “spills over” the edge of the reflector and is lost.

We saw in Sec. 16.4 that the aperture gain is given in terms of the geometrical area  $A$  of the aperture and the aperture-taper and phase-error efficiencies by:

$$G_a = \frac{4\pi A}{\lambda^2} e_{\text{atl}} e_{\text{pel}} \quad (17.8.8)$$

It follows that the reflector antenna gain can be written as:

$$G_{\text{ant}} = G_a e_{\text{spl}} = \frac{4\pi A}{\lambda^2} e_{\text{atl}} e_{\text{pel}} e_{\text{spl}} \quad (17.8.9)$$

The total aperture efficiency is  $e_a = e_{\text{atl}} e_{\text{pel}} e_{\text{spl}}$ . In practice, additional efficiency or loss factors must be introduced, such as those due to cross polarization or to partial aperture blockage by the feed.

Of all the loss factors, the ATL and SPL are the primary ones that significantly affect the gain. Their tradeoff is captured by the *illumination efficiency* or *loss*, defined to be the product of ATL and SPL,  $e_{\text{ill}} = e_{\text{atl}} e_{\text{spl}}$ .

The ATL and SPL may be expressed in terms of the radiation intensity  $U_{\text{feed}}(\psi, \chi)$ . Using  $\rho d\rho = R^2 \sin \psi d\psi = \rho R d\psi = 2FR \tan(\psi/2) d\psi$  and Eq. (17.8.2), we have:

$$|E_a| dA = \sqrt{2\eta U_{\text{feed}}} \frac{1}{R} 2FR \tan \frac{\psi}{2} d\psi d\chi = 2F \sqrt{2\eta U_{\text{feed}}} \tan \frac{\psi}{2} d\psi d\chi$$

$$|E_a|^2 dA = 2\eta U_{\text{feed}} \frac{1}{R^2} R^2 \sin \psi d\psi d\chi = 2\eta U_{\text{feed}} \sin \psi d\psi d\chi$$

The aperture area is  $A = \pi a^2 = \pi(2F)^2 \tan^2(\psi_0/2)$ . Thus, it follows from the definition (16.6.13) that the ATL will be:

$$e_{\text{atl}} = \frac{\left| \int_A |E_a| dA \right|^2}{A \int_A |E_a|^2 dA} = \frac{(2F)^2 \left| \int_A \sqrt{2\eta U_{\text{feed}}} \tan \frac{\psi}{2} d\psi d\chi \right|^2}{\pi (2F)^2 \tan^2(\psi_0/2) \int_A 2\eta U_{\text{feed}} \sin \psi d\psi d\chi}, \quad \text{or,}$$

$$e_{\text{atl}} = \frac{1}{\pi} \cot^2\left(\frac{\psi_0}{2}\right) \frac{\left| \int_0^{\psi_0} \int_0^{2\pi} \sqrt{U_{\text{feed}}(\psi, \chi)} \tan \frac{\psi}{2} d\psi d\chi \right|^2}{\int_0^{\psi_0} \int_0^{2\pi} U_{\text{feed}}(\psi, \chi) \sin \psi d\psi d\chi} \quad (17.8.10)$$

Similarly, the spillover efficiency can be expressed as:

$$e_{\text{spl}} = \frac{P_a}{P_{\text{feed}}} = \frac{\int_0^{\psi_0} \int_0^{2\pi} U_{\text{feed}}(\psi, \chi) \sin \psi d\psi d\chi}{\int_0^{\pi} \int_0^{2\pi} U_{\text{feed}}(\psi, \chi) \sin \psi d\psi d\chi} \quad (17.8.11)$$

where we replaced  $P_{\text{feed}}$  by the integral of  $U_{\text{feed}}$  over all solid angles. It follows that the illumination efficiency  $e_{\text{ill}} = e_{\text{atl}} e_{\text{spl}}$  will be:

$$e_{\text{ill}} = \frac{1}{\pi} \cot^2\left(\frac{\psi_0}{2}\right) \frac{\left| \int_0^{\psi_0} \int_0^{2\pi} \sqrt{U_{\text{feed}}(\psi, \chi)} \tan \frac{\psi}{2} d\psi d\chi \right|^2}{\int_0^{\pi} \int_0^{2\pi} U_{\text{feed}}(\psi, \chi) \sin \psi d\psi d\chi} \quad (17.8.12)$$

An example of a feed pattern that approximates practical patterns is the following azimuthally symmetric radiation intensity [21]:

$$U_{\text{feed}}(\psi, \chi) = \begin{cases} U_0 \cos^4 \psi, & \text{if } 0 \leq \psi \leq \frac{\pi}{2} \\ 0, & \text{if } \frac{\pi}{2} < \psi \leq \pi \end{cases} \quad (17.8.13)$$

For this example, the SPL, ATL, and ILL can be computed in closed form:

$$e_{\text{spl}} = 1 - \cos^5 \psi_0$$

$$e_{\text{atl}} = 40 \cot^2(\psi_0/2) \frac{[\sin^4(\psi_0/2) + \ln(\cos(\psi_0/2))]^2}{1 - \cos^5 \psi_0} \quad (17.8.14)$$

$$e_{\text{ill}} = 40 \cot^2(\psi_0/2) [\sin^4(\psi_0/2) + \ln(\cos(\psi_0/2))]^2$$

The edge illumination is from Eq. (17.8.4):

$$\frac{|E_a(\psi_0)|}{|E_a(0)|} = \frac{1 + \cos \psi_0}{2} \cos^2 \psi_0 \quad (17.8.15)$$

Fig. 17.8.1 shows a plot of Eqs. (17.8.14) and (17.8.15) versus  $\psi_0$ . The ATL is a decreasing and the SPL an increasing function of  $\psi_0$ . The product  $e_{\text{ill}} = e_{\text{atl}} e_{\text{spl}}$  reaches

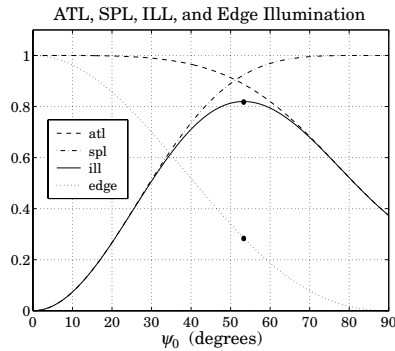


Fig. 17.8.1 Tradeoff between ATL and SPF.

the maximum value of 0.82 at  $\psi_0 = 53.31^\circ$ . The corresponding edge illumination is 0.285 or  $-10.9$  dB. The  $F/D$  ratio is  $\cot(\psi_0/2)/4 = 0.498$ .

This example gives rise to the rule of thumb that the best tradeoff between ATL and SPL for parabolic reflectors is achieved when the edge illumination is about  $-11$  dB.

The value 0.82 for the efficiency is an overestimate. Taking into account other losses, the aperture efficiency of practical parabolic reflectors is typically of the order of 0.55–0.65. Expressing the physical area in terms of the diameter  $D$ , we can summarize the gain of a parabolic antenna:

$$G = e_a \frac{4\pi A}{\lambda^2} = e_a \left( \frac{\pi D}{\lambda} \right)^2, \quad \text{with } e_a = 0.55-0.65 \quad (17.8.16)$$

As we discussed in Sec. 14.3, the 3-dB beamwidth of a reflector antenna with diameter  $D$  can be estimated by rule of thumb [757]:

$$\Delta\theta_{3\text{dB}} = 70^\circ \frac{\lambda}{D} \quad (17.8.17)$$

The beamwidth depends also on the edge illumination. Typically, as the edge attenuation increases, the beamwidth widens and the sidelobes decrease. By studying various reflector sizes, types, and feeds Komen [758] arrived at the following improved approximation for the 3-dB width, which takes into account the edge illumination:

$$\Delta\theta_{3\text{dB}} = (1.05^\circ A_{\text{edge}} + 55.95^\circ) \frac{\lambda}{D} \quad (17.8.18)$$

where  $A_{\text{edge}}$  is the edge attenuation in dB, that is,  $A_{\text{edge}} = -20 \log_{10} [|E_a(\psi_0)/E_a(0)|]$ . For example, for  $A_{\text{edge}} = 11$  dB, the angle factor becomes  $67.5^\circ$ .

### 17.9 Aperture-Field and Current-Distribution Methods

In the previous section, we used energy flow considerations to determine the magnitude  $|E_a|$  of the aperture field. To determine its direction and phase, we need to start from

the field radiated by the feed antenna and trace its path as it propagates as a spherical wave to the reflector surface, gets reflected there, and then propagates as a plane wave along the  $z$ -direction to the aperture plane.

Points on the reflector surface will be parametrized by the spherical coordinates  $R, \psi, \chi$  as shown in Figs. 17.7.1 and 17.7.2, and points in the radiation zone of the reflector antenna, by the usual  $r, \theta, \phi$ .

Let  $\hat{\mathbf{R}}, \hat{\boldsymbol{\psi}}, \hat{\boldsymbol{\chi}}$  be the unit vectors in the  $R, \psi, \chi$  directions. The relationships of  $R, \psi, \chi$  to the conventional polar coordinates of the  $x'y'z'$  coordinate system are:  $R = r', \psi = \theta',$  but  $\chi = -\phi',$  so that the unit vectors are  $\hat{\mathbf{R}} = \hat{\mathbf{r}}', \hat{\boldsymbol{\psi}} = \hat{\boldsymbol{\theta}}',$  and  $\hat{\boldsymbol{\chi}} = -\hat{\boldsymbol{\phi}}'.$  (The primed system has  $\hat{\mathbf{x}}' = \hat{\mathbf{x}}, \hat{\mathbf{y}}' = -\hat{\mathbf{y}},$  and  $\hat{\mathbf{z}}' = -\hat{\mathbf{z}}.$ ) In terms of the unprimed system:

$$\begin{aligned} \hat{\mathbf{R}} &= \hat{\mathbf{x}} \sin \psi \cos \chi + \hat{\mathbf{y}} \sin \psi \sin \chi - \hat{\mathbf{z}} \cos \psi \\ \hat{\boldsymbol{\psi}} &= \hat{\mathbf{x}} \cos \psi \cos \chi + \hat{\mathbf{y}} \cos \psi \sin \chi + \hat{\mathbf{z}} \sin \psi \\ \hat{\boldsymbol{\chi}} &= -\hat{\mathbf{x}} \sin \chi + \hat{\mathbf{y}} \cos \chi \end{aligned} \quad (17.9.1)$$

and conversely,

$$\begin{aligned} \hat{\mathbf{x}} &= \hat{\mathbf{R}} \sin \psi \cos \chi + \hat{\boldsymbol{\psi}} \cos \psi \cos \chi - \hat{\boldsymbol{\chi}} \sin \chi \\ \hat{\mathbf{y}} &= \hat{\mathbf{R}} \sin \psi \sin \chi + \hat{\boldsymbol{\psi}} \cos \psi \sin \chi + \hat{\boldsymbol{\chi}} \cos \chi \\ \hat{\mathbf{z}} &= -\hat{\mathbf{R}} \cos \psi + \hat{\boldsymbol{\psi}} \sin \psi \end{aligned} \quad (17.9.2)$$

Because the reflector is assumed to be in the radiation zone of the feed, the most general field radiated by the feed, and incident at the point  $R, \psi, \chi$  on the reflector surface, will have the form:

$$\mathbf{E}_i = \frac{e^{-jkR}}{R} \mathbf{f}_i(\psi, \chi) \quad (\text{incident field}) \quad (17.9.3)$$

Because of the requirement  $\hat{\mathbf{R}} \cdot \mathbf{E}_i = 0,$  the vector function  $\mathbf{f}_i$  must satisfy  $\hat{\mathbf{R}} \cdot \mathbf{f}_i = 0.$  As expected for radiation fields, the radial dependence on  $R$  is decoupled from the angular dependence on  $\psi, \chi.$  The corresponding magnetic field will be:

$$\mathbf{H}_i = \frac{1}{\eta} \hat{\mathbf{R}} \times \mathbf{E}_i = \frac{1}{\eta} \frac{e^{-jkR}}{R} \hat{\mathbf{R}} \times \mathbf{f}_i(\psi, \chi) \quad (17.9.4)$$

The feed's radiation intensity  $U_{\text{feed}}$  is related to  $\mathbf{f}_i$  through the definition:

$$U_{\text{feed}}(\psi, \chi) = R^2 \frac{1}{2\eta} |\mathbf{E}_i|^2 = \frac{1}{2\eta} |\mathbf{f}_i(\psi, \chi)|^2 \quad (17.9.5)$$

Assuming that the incident field is reflected locally like a plane wave from the reflector's perfectly conducting surface, it follows that the reflected fields  $\mathbf{E}_r, \mathbf{H}_r$  must satisfy the following relationships, where  $\hat{\mathbf{n}}$  is the normal to the reflector:

$$\begin{aligned} \hat{\mathbf{n}} \times \mathbf{E}_r &= -\hat{\mathbf{n}} \times \mathbf{E}_i, & \hat{\mathbf{n}} \cdot \mathbf{E}_r &= \hat{\mathbf{n}} \cdot \mathbf{E}_i \\ \hat{\mathbf{n}} \times \mathbf{H}_r &= \hat{\mathbf{n}} \times \mathbf{H}_i, & \hat{\mathbf{n}} \cdot \mathbf{H}_r &= -\hat{\mathbf{n}} \cdot \mathbf{H}_i \end{aligned} \quad (17.9.6)$$

These imply that  $|\mathbf{E}_r| = |\mathbf{E}_i|, |\mathbf{H}_r| = |\mathbf{H}_i|,$  and that:

$$\begin{aligned} \mathbf{E}_r &= -\mathbf{E}_i + 2\hat{\mathbf{n}}(\hat{\mathbf{n}} \cdot \mathbf{E}_i) \\ \mathbf{H}_r &= \mathbf{H}_i - 2\hat{\mathbf{n}}(\hat{\mathbf{n}} \cdot \mathbf{H}_i) \end{aligned} \quad (17.9.7)$$

Thus, the net electric field  $\mathbf{E}_i + \mathbf{E}_r$  is normal to the surface. Fig. 17.9.1 depicts these geometric relationships, assuming for simplicity that  $\mathbf{E}_i$  is parallel to  $\hat{\boldsymbol{\psi}}$ .

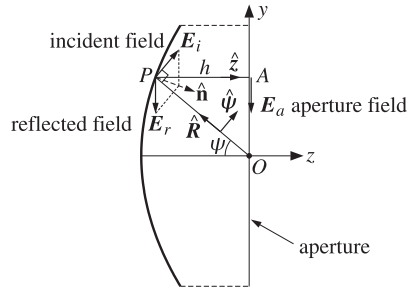


Fig. 17.9.1 Geometric relationship between incident and reflected electric fields.

The proof of Eq. (17.9.7) is straightforward. Indeed, using  $\hat{\mathbf{n}} \times (\mathbf{E}_i + \mathbf{E}_r) = 0$  and the BAC-CAB rule, we have:

$$0 = (\hat{\mathbf{n}} \times (\mathbf{E}_i + \mathbf{E}_r)) \times \hat{\mathbf{n}} = \mathbf{E}_i + \mathbf{E}_r - \hat{\mathbf{n}}(\hat{\mathbf{n}} \cdot \mathbf{E}_i + \hat{\mathbf{n}} \cdot \mathbf{E}_r) = \mathbf{E}_i + \mathbf{E}_r - \hat{\mathbf{n}}(2\hat{\mathbf{n}} \cdot \mathbf{E}_i)$$

It follows now that the reflected field at the point  $(R, \psi, \chi)$  will have the form:

$$\mathbf{E}_r = \frac{e^{-jkR}}{R} \mathbf{f}_r(\psi, \chi) \quad (\text{reflected field}) \quad (17.9.8)$$

where  $\mathbf{f}_r$  satisfies  $|\mathbf{f}_r| = |\mathbf{f}_i|$  and:

$$\mathbf{f}_r = -\mathbf{f}_i + 2\hat{\mathbf{n}}(\hat{\mathbf{n}} \cdot \mathbf{f}_i) \quad (17.9.9)$$

The condition  $\hat{\mathbf{R}} \cdot \mathbf{f}_i = 0$  implies that  $\hat{\mathbf{z}} \cdot \mathbf{f}_r = 0$ , so that  $\mathbf{f}_r$  and  $\mathbf{E}_r$  are perpendicular to the z-axis, and parallel to the aperture plane. To see this, we note that the normal  $\hat{\mathbf{n}}$ , bisecting the angle  $\angle OPA$  in Fig. 17.9.1, will form an angle of  $\psi/2$  with the z axis, so that  $\hat{\mathbf{z}} \cdot \hat{\mathbf{n}} = \cos(\psi/2)$ . More explicitly, the vector  $\hat{\mathbf{n}}$  can be expressed in the form:

$$\hat{\mathbf{n}} = -\hat{\mathbf{R}} \cos \frac{\psi}{2} + \hat{\boldsymbol{\psi}} \sin \frac{\psi}{2} = \hat{\mathbf{z}} \cos \frac{\psi}{2} - (\hat{\mathbf{x}} \cos \chi + \hat{\mathbf{y}} \sin \chi) \sin \frac{\psi}{2} \quad (17.9.10)$$

Then, using Eq. (17.9.2), it follows that:

$$\begin{aligned} \hat{\mathbf{z}} \cdot \mathbf{f}_r &= -\hat{\mathbf{z}} \cdot \mathbf{f}_i + 2(\hat{\mathbf{z}} \cdot \hat{\mathbf{n}})(\hat{\mathbf{n}} \cdot \mathbf{f}_i) \\ &= -(-\hat{\mathbf{R}} \cos \psi + \hat{\boldsymbol{\psi}} \sin \psi) \cdot \mathbf{f}_i + 2 \cos \frac{\psi}{2} (-\hat{\mathbf{R}} \cos \frac{\psi}{2} + \hat{\boldsymbol{\psi}} \sin \frac{\psi}{2}) \cdot \mathbf{f}_i \\ &= -(\hat{\boldsymbol{\psi}} \cdot \mathbf{f}_i) \left[ \sin \psi - 2 \cos \frac{\psi}{2} \sin \frac{\psi}{2} \right] = 0 \end{aligned}$$

Next, we obtain the aperture field  $\mathbf{E}_a$  by propagating  $\mathbf{E}_r$  as a plane wave along the z-direction by a distance  $h$  to the aperture plane:

$$\mathbf{E}_a = e^{-jkh} \mathbf{E}_r = \frac{e^{-jk(R+h)}}{R} \mathbf{f}_r(\psi, \chi)$$

But for the parabola, we have  $R + h = 2F$ . Thus, the aperture field is given by:

$$\mathbf{E}_a = \frac{e^{-2jkF}}{R} \mathbf{f}_a(\psi, \chi) \quad (\text{aperture field}) \quad (17.9.11)$$

where we defined  $\mathbf{f}_a = \mathbf{f}_r$ , so that:

$$\mathbf{f}_a = -\mathbf{f}_i + 2\hat{\mathbf{n}}(\hat{\mathbf{n}} \cdot \mathbf{f}_i) \quad (17.9.12)$$

Because  $|\mathbf{f}_a| = |\mathbf{f}_r| = |\mathbf{f}_i| = \sqrt{2\eta U_{\text{feed}}}$ , it follows that Eq. (17.9.11) is consistent with Eq. (17.8.2). As plane waves propagating in the z-direction, the reflected and aperture fields are Huygens sources. Therefore, the corresponding magnetic fields will be:

$$\mathbf{H}_r = \frac{1}{\eta} \hat{\mathbf{z}} \times \mathbf{E}_r, \quad \mathbf{H}_a = \frac{1}{\eta} \hat{\mathbf{z}} \times \mathbf{E}_a$$

The surface currents induced on the reflector are obtained by noting that the total fields are  $\mathbf{E}_i + \mathbf{E}_r = 2\hat{\mathbf{n}}(\hat{\mathbf{n}} \cdot \mathbf{E}_i)$  and  $\mathbf{H}_i + \mathbf{H}_r = 2\mathbf{H}_i - 2\hat{\mathbf{n}}(\hat{\mathbf{n}} \cdot \mathbf{H}_i)$ . Thus, we have:

$$\mathbf{J}_s = \hat{\mathbf{n}} \times (\mathbf{H}_i + \mathbf{H}_r) = 2\hat{\mathbf{n}} \times \mathbf{H}_i = \frac{2}{\eta} \frac{e^{-jkR}}{R} \hat{\mathbf{R}} \times \mathbf{f}_i$$

$$\mathbf{J}_{ms} = -\hat{\mathbf{n}} \times (\mathbf{E}_i + \mathbf{E}_r) = 0$$

## 17.10 Radiation Patterns of Reflector Antennas

The radiation patterns of the reflector antenna are obtained either from the aperture fields  $\mathbf{E}_a, \mathbf{H}_a$  integrated over the effective aperture using Eq. (16.4.2), or from the currents  $\mathbf{J}_s$  and  $\mathbf{J}_{ms} = 0$  integrated over the curved reflector surface using Eq. (16.4.1).

We discuss in detail only the aperture-field case. The radiation fields at some large distance  $r$  in the direction defined by the polar angles  $\theta, \phi$  are given by Eq. (16.5.3). The unit vector  $\hat{\mathbf{r}}$  in the direction of  $\theta, \phi$  is shown in Fig. 17.7.2. We have:

$$E_\theta = jk \frac{e^{-jkr}}{2\pi r} \frac{1 + \cos \theta}{2} [f_x \cos \phi + f_y \sin \phi] \quad (17.10.1)$$

$$E_\phi = jk \frac{e^{-jkr}}{2\pi r} \frac{1 + \cos \theta}{2} [f_y \cos \phi - f_x \sin \phi]$$

where the vector  $\mathbf{f} = \hat{\mathbf{x}} f_x + \hat{\mathbf{y}} f_y$  is the Fourier transform over the aperture:

$$\mathbf{f}(\theta, \phi) = \int_0^a \int_0^{2\pi} \mathbf{E}_a(\rho', \chi) e^{jk\mathbf{r}' \cdot \boldsymbol{\rho}'} d\rho' d\chi \quad (17.10.2)$$



The vector  $\mathbf{r}'$  lies on the aperture plane and is given in cylindrical coordinates by  $\mathbf{r}' = \rho' \hat{\rho} = \rho' (\hat{\mathbf{x}} \cos \chi + \hat{\mathbf{y}} \sin \chi)$ . Thus,

$$\begin{aligned} \mathbf{k} \cdot \mathbf{r}' &= k\rho' (\hat{\mathbf{x}} \cos \phi \sin \theta + \hat{\mathbf{y}} \sin \phi \sin \theta + \hat{\mathbf{z}} \cos \theta) \cdot (\hat{\mathbf{x}} \cos \chi + \hat{\mathbf{y}} \sin \chi) \\ &= k\rho' \sin \theta (\cos \phi \cos \chi + \sin \phi \sin \chi) = k\rho' \sin \theta \cos(\phi - \chi) \end{aligned}$$

It follows that:

$$\mathbf{f}(\theta, \phi) = \int_0^a \int_0^{2\pi} \mathbf{E}_a(\rho, \chi) e^{jk\rho \sin \theta \cos(\phi - \chi)} \rho d\rho d\chi \quad (17.10.3)$$

We may convert this into an integral over the feed angles  $\psi, \chi$  by using Eq. (17.9.11) and  $d\rho = R d\psi$ ,  $\rho = 2F \tan(\psi/2)$ , and  $\rho d\rho = 2FR \tan(\psi/2) d\psi$ . Then, the  $1/R$  factor in  $\mathbf{E}_a$  is canceled, resulting in:

$$\mathbf{f}(\theta, \phi) = 2Fe^{-2jkF} \int_0^{\psi_0} \int_0^{2\pi} \mathbf{f}_a(\psi, \chi) e^{2jkF \tan \frac{\psi}{2} \sin \theta \cos(\phi - \chi)} \tan \frac{\psi}{2} d\psi d\chi \quad (17.10.4)$$

Given a feed pattern  $\mathbf{f}_i(\psi, \chi)$ , the aperture pattern  $\mathbf{f}_a(\psi, \chi)$  is determined from Eq. (17.9.12) and the integrations in (17.10.4) are done numerically.

Because of the condition  $\hat{\mathbf{R}} \cdot \mathbf{f}_i = 0$ , the vector  $\mathbf{f}_i$  will have components only along the  $\hat{\boldsymbol{\psi}}$  and  $\hat{\boldsymbol{\chi}}$  directions. We assume that  $\mathbf{f}_i$  has the following more specific form:

$$\mathbf{f}_i = \hat{\boldsymbol{\psi}} F_1 \sin \chi + \hat{\boldsymbol{\chi}} F_2 \cos \chi \quad (y\text{-polarized feeds}) \quad (17.10.5)$$

where  $F_1, F_2$  are functions of  $\psi, \chi$ , but often assumed to be functions only of  $\psi$ , representing the patterns along the principal planes  $\chi = 90^\circ$  and  $\chi = 0^\circ$ .

Such feeds are referred to as “ $y$ -polarized” and include  $y$ -directed dipoles, and waveguides and horns in which the electric field on the horn aperture is polarized along the  $y$  direction (the  $x$ -polarized case is obtained by a rotation, replacing  $\chi$  by  $\chi + 90^\circ$ ). Using Eqs. (17.9.1) and (17.9.10), the corresponding pattern  $\mathbf{f}_a$  can be worked out:

$$\mathbf{f}_a = -\hat{\mathbf{y}} [F_1 \sin^2 \chi + F_2 \cos^2 \chi] - \hat{\mathbf{x}} [(F_1 - F_2) \cos \chi \sin \chi] \quad (17.10.6)$$

If  $F_1 = F_2$ , we have  $\mathbf{f}_a = -\hat{\mathbf{y}} F_1$ . But if  $F_1 \neq F_2$ , the aperture field  $\mathbf{E}_a$  develops a “cross-polarized” component along the  $x$  direction. Various definitions of cross polarization have been discussed by Ludwig [763].

As examples, we consider the cases of a  $y$ -directed Hertzian dipole feed, and waveguide and horn feeds. Adapting their radiation patterns given in Sections 15.2, 17.1, and 17.3, to the  $R, \psi, \chi$  coordinate system, we obtain the following feed patterns, which are special cases of (17.10.5):

$$\begin{aligned} \mathbf{f}_i(\psi, \chi) &= F_d (\hat{\boldsymbol{\psi}} \cos \psi \sin \chi + \hat{\boldsymbol{\chi}} \cos \chi) && \text{(dipole feed)} \\ \mathbf{f}_i(\psi, \chi) &= F_w(\psi, \chi) (\hat{\boldsymbol{\psi}} \sin \chi + \hat{\boldsymbol{\chi}} \cos \chi) && \text{(waveguide feed)} \\ \mathbf{f}_i(\psi, \chi) &= F_h(\psi, \chi) (\hat{\boldsymbol{\psi}} \sin \chi + \hat{\boldsymbol{\chi}} \cos \chi) && \text{(horn feed)} \end{aligned} \quad (17.10.7)$$

where  $F_d$  is the constant  $F_d = -j\eta(I\ell)/2\lambda$ , and  $F_w, F_h$  are given by:

$$F_w(\psi, \chi) = -\frac{jabE_0}{\pi\lambda} (1 + \cos \psi) \frac{\cos(\pi v_x)}{1 - 4v_x^2} \frac{\sin(\pi v_y)}{\pi v_y} \quad (17.10.8)$$

$$F_h(\psi, \chi) = -\frac{jABE_0}{8\lambda} (1 + \cos \psi) F_1(v_x, \sigma_a) F_0(v_y, \sigma_b)$$

where  $I, \ell$  are the current and length of the Hertzian dipole,  $a, b$  and  $A, B$  are the dimensions of the waveguide and horn apertures, and  $v_x = (a/\lambda) \sin \psi \cos \chi$ ,  $v_y = (b/\lambda) \sin \psi \sin \chi$  for the waveguide, and  $v_x = (A/\lambda) \sin \psi \cos \chi$ ,  $v_y = (B/\lambda) \sin \psi \sin \chi$ , for the horn, and  $F_1, F_0$  are the horn pattern functions defined in Sec. 17.3. The corresponding aperture patterns  $\mathbf{f}_a$  are in the three cases:

$$\begin{aligned} \mathbf{f}_a(\psi, \chi) &= -\hat{\mathbf{y}} F_d [\cos \psi \sin^2 \chi + \cos^2 \chi] - \hat{\mathbf{x}} F_d [(\cos \psi - 1) \sin \chi \cos \chi] \\ \mathbf{f}_a(\psi, \chi) &= -\hat{\mathbf{y}} F_w(\psi, \chi) \\ \mathbf{f}_a(\psi, \chi) &= -\hat{\mathbf{y}} F_h(\psi, \chi) \end{aligned} \quad (17.10.9)$$

In the general case, a more convenient form of Eq. (17.10.6) is obtained by writing it in terms of the sum and difference patterns:

$$A = \frac{F_1 + F_2}{2}, \quad B = \frac{F_1 - F_2}{2} \quad \Leftrightarrow \quad F_1 = A + B, \quad F_2 = A - B \quad (17.10.10)$$

Using some trigonometric identities, we may write (17.10.6) in the form:

$$\mathbf{f}_a = -\hat{\mathbf{y}} (A - B \cos 2\chi) - \hat{\mathbf{x}} (B \sin 2\chi) \quad (17.10.11)$$

In general,  $A, B$  will be functions of  $\psi, \chi$  (as in the waveguide and horn cases.) If we assume that they are functions only of  $\psi$ , then the  $\chi$ -integration in the radiation pattern integral (17.10.4) can be done explicitly leaving an integral over  $\psi$  only. Using (17.10.11) and the Bessel-function identities,

$$\int_0^{2\pi} e^{ju \cos(\phi - \chi)} \begin{bmatrix} \cos n\chi \\ \sin n\chi \end{bmatrix} d\chi = 2\pi j^n \begin{bmatrix} \cos n\phi \\ \sin n\phi \end{bmatrix} J_n(u) \quad (17.10.12)$$

we obtain:

$$\mathbf{f}(\theta, \phi) = -\hat{\mathbf{y}} [f_A(\theta) - f_B(\theta) \cos 2\phi] - \hat{\mathbf{x}} [f_B(\theta) \sin 2\phi] \quad (17.10.13)$$

where the functions  $f_A(\theta)$  and  $f_B(\theta)$  are defined by:

$$\begin{aligned} f_A(\theta) &= 4\pi F e^{-2jkF} \int_0^{\psi_0} A(\psi) J_0 \left( \frac{4\pi F}{\lambda} \tan \frac{\psi}{2} \sin \theta \right) \tan \frac{\psi}{2} d\psi \\ f_B(\theta) &= -4\pi F e^{-2jkF} \int_0^{\psi_0} B(\psi) J_2 \left( \frac{4\pi F}{\lambda} \tan \frac{\psi}{2} \sin \theta \right) \tan \frac{\psi}{2} d\psi \end{aligned} \quad (17.10.14)$$

Using Eq. (17.10.13) and some trigonometric identities, we obtain:

$$\begin{aligned} f_x \cos \phi + f_y \sin \phi &= -(f_A + f_B) \sin \phi \\ f_y \cos \phi - f_x \sin \phi &= -(f_A - f_B) \cos \phi \end{aligned}$$

It follows that the radiation fields (17.10.1) are given by:

$$\begin{aligned} E_\theta &= -j \frac{e^{-jkr}}{\lambda r} \frac{1 + \cos \theta}{2} [f_A(\theta) + f_B(\theta)] \sin \phi \\ E_\phi &= -j \frac{e^{-jkr}}{\lambda r} \frac{1 + \cos \theta}{2} [f_A(\theta) - f_B(\theta)] \cos \phi \end{aligned} \quad (17.10.15)$$

**Example 17.10.1:** *Parabolic Reflector with Hertzian Dipole Feed.* We compute numerically the gain patterns for a  $y$ -directed Hertzian dipole feed. We take  $F = 10\lambda$  and  $D = 40\lambda$ , so that  $F/D = 0.25$  and  $\psi_0 = 90^\circ$ . These choices are similar to those in [761].

Ignoring the constant  $F_d$  in (17.10.7), we have  $F_1(\psi) = \cos \psi$  and  $F_2(\psi) = 1$ . Thus, the sum and difference patterns are  $A(\psi) = (\cos \psi + 1)/2$  and  $B(\psi) = (\cos \psi - 1)/2$ . Up to some overall constants, the required gain integrals will have the form:

$$f_A(\theta) = \int_0^{\psi_0} F_A(\psi, \theta) d\psi, \quad f_B(\theta) = \int_0^{\psi_0} F_B(\psi, \theta) d\psi \quad (17.10.16)$$

where

$$\begin{aligned} F_A(\psi, \theta) &= (1 + \cos \psi) J_0 \left( \frac{4\pi F}{\lambda} \tan \frac{\psi}{2} \sin \theta \right) \tan \frac{\psi}{2} \\ F_B(\psi, \theta) &= (1 - \cos \psi) J_2 \left( \frac{4\pi F}{\lambda} \tan \frac{\psi}{2} \sin \theta \right) \tan \frac{\psi}{2} \end{aligned} \quad (17.10.17)$$

The integrals are evaluated numerically using Gauss-Legendre quadrature integration, which approximates an integral as a weighted sum [103]:

$$f_A(\theta) = \sum_{i=1}^N w_i F_A(\psi_i, \theta) = \mathbf{w}^T \mathbf{F}_A$$

where  $w_i, \psi_i$  are the Gauss-Legendre weights and evaluation points within the integration interval  $[0, \psi_0]$ , where  $\mathbf{F}_A$  is the column vector with  $i$ th component  $F_A(\psi_i, \theta)$ .

For higher accuracy, this interval may be subdivided into a number of subintervals, the quantities  $w_i, \psi_i$  are then determined on each subinterval, and the total integral is evaluated as the sum of the integrals over all the subintervals.

We have written a MATLAB function, `quadrs`, that determines the quantities  $w_i, \psi_i$  over all the subintervals. It is built on the function `quadr`, which determines the weights over a single interval.

The following MATLAB code evaluates and plots in Fig. 17.10.1 the  $E$ - and  $H$ -plane patterns (17.10.15) over the polar angles  $0 \leq \theta \leq 5^\circ$ .

```
F = 10; D = 40; psi0 = 2*acot(4*F/D); % F/D = 0.25, psi0 = 90°
ab = linspace(0, psi0, 5); % 4 integration subintervals in [0, psi0]
[w,psi] = quadrs(ab); % quadrature weights and evaluation points
% uses 16 weights per subinterval
c = cos(psi); t = tan(psi/2); % cos psi, tan(psi/2) at quadrature points
th = linspace(0, 5, 251); % angle theta in degrees over 0 ≤ theta ≤ 5°
for i=1:length(th),
    u = 4*pi*F*sin(th(i)*pi/180); % u = 2kF sin theta
```

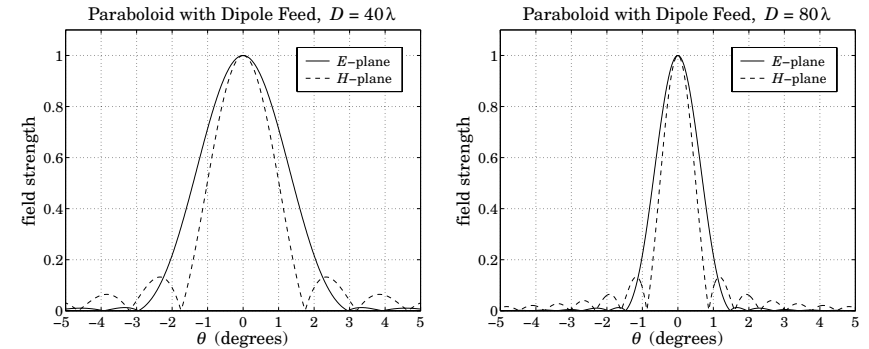


Fig. 17.10.1 Parabolic reflector patterns with dipole feed.

```
FA = (1+c) .* besselj(0, u*t) .* t; % integrand of fA(theta)
fA(i) = w' * FA; % integral evaluated at theta
FB = (1-c) .* besselj(2, u*t) .* t; % integrand of fB(theta)
fB(i) = w' * FB;
end
gh = abs((1+cos(th)).*(fA-fB)); gh = gh/max(gh); % gain patterns
ge = abs((1+cos(th)).*(fA+fB)); ge = ge/max(ge);
plot(-thd,ge,'-', thd,ge, '-.', -thd,gh,'--', thd,gh,'--');
```

The graph on the right has  $\psi_0 = 90^\circ$  and  $D = 80\lambda$ , resulting in a narrower main beam. □

**Example 17.10.2:** *Parabolic Reflector with Waveguide Feed.* We calculate the reflector radiation patterns for a waveguide feed radiating in the  $TE_{10}$  mode with a  $y$ -directed electric field. The feed pattern was given in Eq. (17.10.7). Ignoring some overall constants, we have with  $v_x = (a/\lambda) \sin \psi \cos \chi$  and  $v_y = (b/\lambda) \sin \psi \sin \chi$ :

$$f_i = (1 + \cos \psi) \frac{\cos(\pi v_x)}{1 - 4v_x^2} \frac{\sin(\pi v_y)}{\pi v_y} (\hat{\psi} \sin \chi + \hat{\chi} \cos \chi) \quad (17.10.18)$$

To avoid the double integration in the  $\psi$  and  $\chi$  variables, we follow Jones' procedure [761] of choosing the  $a, b$  such that the  $E$ - and  $H$ -plane illuminations of the paraboloid are essentially identical. This is accomplished when  $a$  is approximately  $a = 1.37b$ . Then, the above feed pattern may be simplified by replacing it by its  $E$ -plane pattern:

$$f_i = (1 + \cos \psi) \frac{\sin(\pi v_y)}{\pi v_y} (\hat{\psi} \sin \chi + \hat{\chi} \cos \chi) \quad (17.10.19)$$

where  $v_y = (b/\lambda) \sin \psi$ . Thus,  $F_1 = F_2$  and

$$A(\psi) = (1 + \cos \psi) \frac{\sin(\pi b \sin \psi / \lambda)}{\pi b \sin \psi / \lambda} \quad \text{and} \quad B(\psi) = 0 \quad (17.10.20)$$

The radiated field is given by Eq. (17.10.15) with a normalized gain:

$$g(\theta) = \left| \frac{1 + \cos \theta}{2} \frac{f_A(\theta)}{f_A(0)} \right|^2 \quad (17.10.21)$$

where  $f_A(\theta)$  is defined up to a constant by Eq. (17.10.14):

$$f_A(\theta) = \int_0^{\psi_0} A(\psi) J_0\left(\frac{4\pi F}{\lambda} \tan\frac{\psi}{2} \sin\theta\right) \tan\frac{\psi}{2} d\psi \quad (17.10.22)$$

We choose a parabolic antenna with diameter  $D = 40\lambda$  and subtended angle of  $\psi_0 = 60^\circ$ , so that  $F = D \cot(\psi_0/2)/4 = 17.3205\lambda$ . The length  $b$  of the waveguide is chosen such as to achieve an edge illumination of  $-11$  dB on the paraboloid. This gives the condition on  $b$ , where the extra factor of  $(1 + \cos\psi)$  arises from the space attenuation factor  $1/R$ :

$$\frac{|E_i(\psi_0)|}{|E_i(0)|} = \left(\frac{1 + \cos\psi_0}{2}\right)^2 \left|\frac{\sin(\pi b \sin\psi_0/\lambda)}{\pi b \sin\psi_0/\lambda}\right| = 10^{-11/20} = 0.2818 \quad (17.10.23)$$

It has solution  $b = 0.6958\lambda$  and therefore,  $a = 1.37b = 0.9533\lambda$ . The illumination efficiency given in Eq. (17.8.12) may be taken to be a measure of the overall aperture efficiency of the reflector. Because  $2\eta U_{\text{feed}} = |f_i|^2 = |f_a|^2 = |A(\psi)|^2$ , the integrals in (17.8.12) may be calculated numerically, giving  $e_a = 0.71$  and a gain of 40.5 dB.

The pattern function  $f_A(\theta)$  may be calculated numerically as in the previous example. The left graph in Fig. 17.10.2 shows the  $E$ - and  $H$ -plane illumination patterns versus  $\psi$  of the actual feed given by (17.10.18), that is, the normalized gains:

$$g_E(\psi) = \left|\frac{(1 + \cos\psi)^2 \sin(\pi b \sin\psi/\lambda)}{4 \pi b \sin\psi/\lambda}\right|^2$$

$$g_H(\psi) = \left|\frac{(1 + \cos\psi)^2 \cos(\pi a \sin\psi/\lambda)}{4 (1 - 4(\pi a \sin\psi/\lambda)^2)}\right|^2$$

They are essentially identical provided  $a = 1.37b$  (the graph actually plots the square roots of these quantities.) The right graph shows the calculated radiation pattern  $g(\theta)$  (or, rather its square root) of the paraboloid.

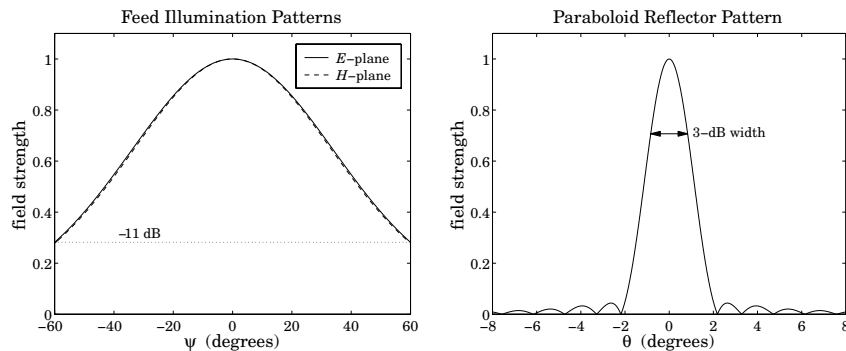


Fig. 17.10.2 Feed illumination and reflector radiation patterns.

The following MATLAB code solves (17.10.23) for  $b$ , and then calculates the illumination pattern and the reflector pattern:

```
F = 17.3205; D = 40; psi0 = 2*acot(4*F/D); % psi0 = 60°
f = inline('(1+cos(x)).^2/4 * abs(sinc(b*sin(x))) - A','b','x','A');
Aedge = 11;
b = fzero(f,0.8,optimset('display','off'), psi0, 10^(-Aedge/20));
a = 1.37 * b;

psi = linspace(-psi0, psi0, 201); ps = psi * 180/pi;

gE = abs((1+cos(psi)).^2/4 .* sinc(b*sin(psi)));
gH = abs((1+cos(psi)).^2/4 .* dsinc(a*sin(psi)));

figure; plot(ps,gE,'-', ps,gH,'--');

[w,psi] = quadrs(linspace(0, psi0, 5)); % quadrature weights and points
s = sin(psi); c = cos(psi); t = tan(psi/2);
A = (1+c) .* sinc(b*s); % the pattern A(psi)

thd = linspace(0, 5, 251); th = thd*pi/180;

for i=1:length(th),
    u = 4*pi*F*sin(th(i));
    FA = A .* besselj(0, u*t) .* t;
    fA(i) = w * FA;
end

g = abs((1+cos(th)) .* fA); g = g/max(g);

figure; plot(-thd,g,'-', thd,g);
```

The 3-dB width was calculated from Eq. (17.8.18) and is placed on the graph. The angle factor was  $1.05A_{\text{edge}} + 55.95 = 67.5$ , so that  $\Delta\theta_{3\text{dB}} = 67.5^\circ\lambda/D = 67.5/40 = 1.69^\circ$ . The gain-beamwidth product is  $p = G(\Delta\theta_{3\text{dB}})^2 = 10^{40.5/10} (1.69^\circ)^2 = 32046 \text{ deg}^2$ . □

**Example 17.10.3: Parabolic Reflector with Horn Feed.** Fig. 17.10.3 shows the illumination and reflector patterns if a rectangular horn antenna feed is used instead of a waveguide. The design requirements were again that the edge illumination be  $-11$  dB and that  $D = 40\lambda$  and  $\psi_0 = 60^\circ$ . The illumination pattern is (up to a scale factor):

$$f_i = (1 + \cos\psi)F_1(v_x, \sigma_a)F_0(v_y, \sigma_b)(\hat{\psi} \sin\chi + \hat{\chi} \cos\chi)$$

The  $E$ - and  $H$ -plane illumination patterns are virtually identical over the angular range  $0 \leq \psi \leq \psi_0$ , provided one chooses the horn sides such that  $A = 1.48B$ . Then, the illumination field may be simplified by replacing it by the  $E$ -plane pattern and the length  $B$  is determined by requiring that the edge illumination be  $-11$  dB. Therefore, we work with:

$$f_i = (1 + \cos\psi)F_0(v_y, \sigma_b)(\hat{\psi} \sin\chi + \hat{\chi} \cos\chi), \quad v_y = \frac{B}{\lambda} \sin\psi$$

Then,  $A(\psi) = (1 + \cos\psi)F_0(v_y, \sigma_b)$  and  $B(\psi) = 0$  for the sum and difference patterns. The edge illumination condition reads now:

$$\left(\frac{1 + \cos\psi_0}{2}\right)^2 \left|\frac{F_0(\pi B \sin\psi_0/\lambda, \sigma_b)}{F_0(0, \sigma_b)}\right| = 10^{-11/20}$$

Its solution is  $B = 0.7806\lambda$ , and hence  $A = 1.48B = 1.1553\lambda$ . The left graph in Fig. 17.10.3 shows the  $E$ - and  $H$ -plane illumination gain patterns of the actual horn feed:

$$g_E(\psi) = \left| \frac{(1 + \cos \psi)^2}{4} \frac{F_0(\pi B \sin \psi_0 / \lambda, \sigma_b)}{F_0(0, \sigma_b)} \right|^2$$

$$g_H(\psi) = \left| \frac{(1 + \cos \psi)^2}{4} \frac{F_1(\pi A \sin \psi_0 / \lambda, \sigma_a)}{F_1(0, \sigma_a)} \right|^2$$

They are seen to be almost identical. The right graph shows the reflector radiation pattern computed numerically as in the previous example. The following MATLAB code illustrates this computation:

```
[w,psi] = quadrs(linspace(0, psi0, 5)); % 4 subintervals in [0,psi0]
s = sin(psi); c = cos(psi); t = tan(psi/2); % evaluate at quadrature points
Apsi = (1+c) .* (diffint(B*s, sb, 0)); % the pattern A(ψ)
thd = linspace(0, 8, 251); th = thd*pi/180;
for i=1:length(th),
    u = 4*pi*f*sin(th(i));
    FA = Apsi .* besselj(0, u*t) .* t;
    fA(i) = w' * FA;
end
g = abs((1+cos(th)) .* fA); g = g/max(g);
figure; plot(-thd,g,'-', thd,g);
```

The horn's  $\sigma$ -parameters were chosen to have the usual optimum values of  $\sigma_a = 1.2593$  and  $\sigma_b = 1.0246$ . The 3-dB width is the same as in the previous example, that is,  $1.69^\circ$  and is shown on the graph. The computed antenna efficiency is now  $e_a = 0.67$  and the corresponding gain 40.24 dB, so that  $p = G(\Delta\theta_{3dB})^2 = 10^{40.24/10} (1.69^\circ)^2 = 30184 \text{ deg}^2$  for the gain-beamwidth product. □

**Example 17.10.4:** Here, we compare the approximate symmetrized patterns of the previous two examples with the exact patterns obtained by performing the double-integration over the aperture variables  $\psi, \chi$ .

Both the waveguide and horn examples have a  $y$ -directed two-dimensional Fourier transform pattern of the form:

$$f_A(\theta, \phi) = f_y(\theta, \phi) = \int_0^{\psi_0} \int_0^{2\pi} F_A(\psi, \chi, \theta, \phi) d\psi d\chi \quad (17.10.24)$$

where the integrand depends on the feed pattern  $A(\psi, \chi)$ :

$$F_A(\psi, \chi, \theta, \phi) = A(\psi, \chi) e^{j2kF \tan(\psi/2) \sin \theta \cos(\phi - \chi)} \tan \frac{\psi}{2} \quad (17.10.25)$$

and, up to constant factors, the function  $A(\psi, \chi)$  is given in the two cases by:

$$A(\psi, \chi) = (1 + \cos \psi) \frac{\cos(\pi v_x)}{1 - 4v_x^2} \frac{\sin(\pi v_y)}{\pi v_y} \quad (17.10.26)$$

$$A(\psi, \chi) = (1 + \cos \psi) F_1(v_x, \sigma_a) F_0(v_y, \sigma_b)$$

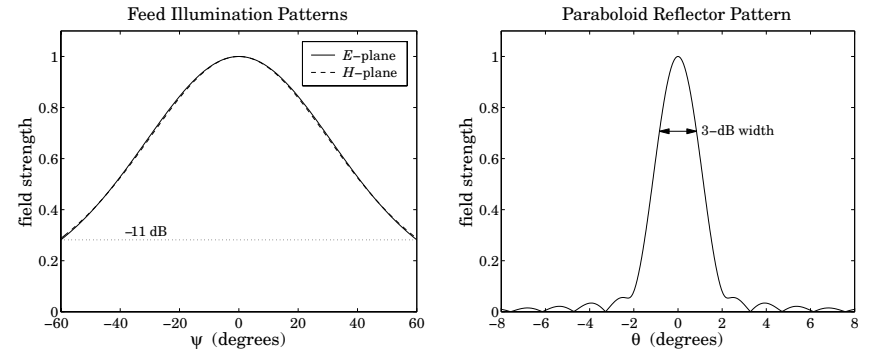


Fig. 17.10.3 Feed and reflector radiation patterns.

where  $v_x = (a/\lambda) \sin \psi \cos \chi$  and  $v_y = (b/\lambda) \sin \psi \sin \chi$  for the waveguide case, and  $v_x = (A/\lambda) \sin \psi \cos \chi$  and  $v_y = (B/\lambda) \sin \psi \sin \chi$  for the horn.

Once,  $f_A(\theta, \phi)$  is computed, we obtain the (un-normalized)  $H$ - and  $E$ -plane radiation patterns for the reflector by setting  $\phi = 0^\circ$  and  $90^\circ$ , that is,

$$g_H(\theta) = |(1 + \cos \theta) f_A(\theta, 0^\circ)|^2, \quad g_E(\theta) = |(1 + \cos \theta) f_A(\theta, 90^\circ)|^2 \quad (17.10.27)$$

The numerical evaluation of Eq. (17.10.24) can be done with two-dimensional Gauss-Legendre quadratures, approximating the integral by the double sum:

$$f_A(\theta, \phi) = \sum_{i=1}^{N_1} \sum_{j=1}^{N_2} w_{1i} F_A(\psi_i, \chi_j) w_{2j} = \mathbf{w}_1^T \mathbf{F}_A \mathbf{w}_2 \quad (17.10.28)$$

where  $\{w_{1i}, \psi_i\}$  and  $\{w_{2j}, \chi_j\}$  are the quadrature weights and evaluation points over the intervals  $[0, \psi_0]$  and  $[0, 2\pi]$ , and  $\mathbf{F}_A$  is the matrix  $F_A(\psi_i, \chi_j)$ . The function `quadr`s, called on these two intervals, will generate these weights.

Fig. 17.10.4 shows the patterns (17.10.27) of the horn and waveguide cases evaluated numerically and plotted together with the approximate symmetrized patterns of the previous two examples. The symmetrized patterns agree very well with the exact patterns and fall between them. The following MATLAB code illustrates this computation for the horn case:

```
[w1, psi] = quadrs(linspace(0, psi0, Ni)); % quadrature over [0,psi0], Nbi = 5
[w2, chi] = quadrs(linspace(0, 2*pi, Ni)); % quadrature over [0,2π], Nbi = 5
sinpsi = sin(psi); cospsi = cos(psi); tanpsi = tan(psi/2);
sinchi = sin(chi); coschi = cos(chi);
for i = 1:length(chi), % build matrix A(ψbi,χbj) columnwise
    Apsi(:,i) = diffint(A*sinpsi*coschi(i), sa, 1) ...
        .* diffint(B*sinpsi*sinchi(i), sb, 0);
end
Apsi = repmat(tanpsi.*(1+cospsi), 1, length(psi)) .* Apsi;
th = linspace(0, 8, 401) * pi/180;
```

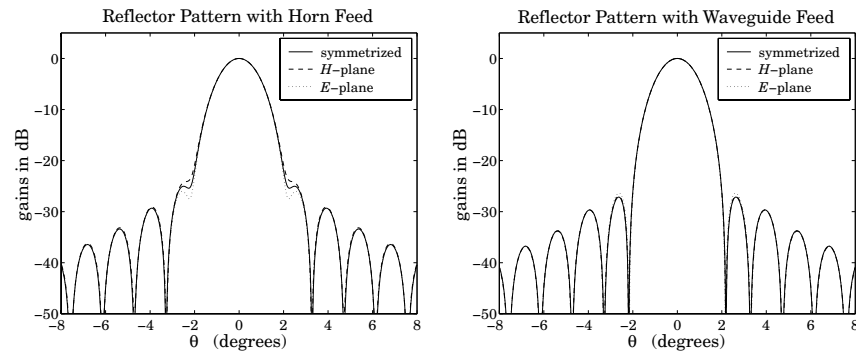


Fig. 17.10.4 Exact and approximate reflector radiation patterns.

```

for i=1:length(th),
    u = 4*pi*F*sin(th(i));
    FH = Apsi .* exp(j*u*tanpsi*coschi');
    FE = Apsi .* exp(j*u*tanpsi*sinchi');
    fH(i) = w1' * FH * w2;
    fE(i) = w1' * FE * w2;
end

gH = abs((1+cos(th)).*fH); gH = gH/max(gH);
gE = abs((1+cos(th)).*fE); gE = gE/max(gE);
    
```

The patterns are plotted in dB, which accentuates the differences among the curves and also shows the sidelobe levels. In the waveguide case the resulting curves are almost indistinguishable to be seen as separate. □

### 17.11 Dual-Reflector Antennas

Dual-reflector antennas consisting of a main reflector and a secondary sub-reflector are used to increase the effective focal length and to provide convenient placement of the feed.

Fig. 17.11.1 shows a Cassegrain antenna<sup>†</sup> consisting of a parabolic reflector and a hyperbolic subreflector. The hyperbola is positioned such that its focus  $F_2$  coincides with the focus of the parabola. The feed is placed at the other focus,  $F_1$ , of the hyperbola.

The focus  $F_2$  is referred to a “virtual focus” of the parabola. Any ray originating from the point  $F_1$  will be reflected by the hyperbola in a direction that appears to have originated from the focus  $F_2$ , and therefore, it will be re-reflected parallel to the parabola’s axis.

To better understand the operation of such an antenna, we consider briefly the reflection properties of hyperbolas and ellipses, as shown in Fig. 17.11.2.

<sup>†</sup>Invented in the 17th century by A. Cassegrain.

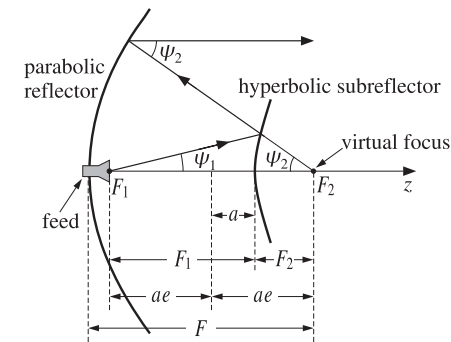


Fig. 17.11.1 Cassegrain dual-reflector antenna.

The geometrical properties of hyperbolas and ellipses are characterized completely by the parameters  $e, a$ , that is, the eccentricity and the distance of the vertices from the origin. The eccentricity is  $e > 1$  for a hyperbola, and  $e < 1$  for an ellipse. A circle corresponds to  $e = 0$  and a parabola can be thought of as the limit of a hyperbola in the limit  $e = 1$ .

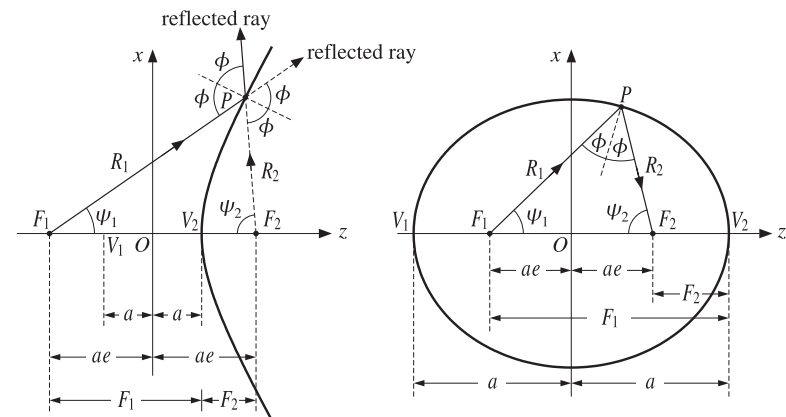


Fig. 17.11.2 Hyperbolic and elliptic reflectors.

The foci are at distances  $F_1$  and  $F_2$  from a vertex, say from the vertex  $V_2$ , and are given in terms of  $a, e$  as follows:

$$\begin{aligned}
 F_1 &= a(e + 1), & F_2 &= a(e - 1) && \text{(hyperbola)} \\
 F_1 &= a(1 + e), & F_2 &= a(1 - e) && \text{(ellipse)}
 \end{aligned}
 \tag{17.11.1}$$

The ray lengths  $R_1$  and  $R_2$  from the foci to a point  $P$  satisfy:

$$\begin{aligned}
 R_1 - R_2 &= 2a && \text{(hyperbola)} \\
 R_1 + R_2 &= 2a && \text{(ellipse)}
 \end{aligned}
 \tag{17.11.2}$$

The polar representations of the hyperbola or ellipse may be given in terms of the polar angles  $\psi_1$  or  $\psi_2$ . We have:

$$R_1 = \frac{a(e^2 - 1)}{e \cos \psi_1 - 1}, \quad R_2 = \frac{a(e^2 - 1)}{e \cos \psi_2 + 1} \quad (\text{hyperbola})$$

$$R_1 = \frac{a(1 - e^2)}{1 - e \cos \psi_1}, \quad R_2 = \frac{a(1 - e^2)}{1 - e \cos \psi_2} \quad (\text{ellipse})$$
(17.11.3)

Note that we can write  $a(e^2 - 1) = F_1(e - 1) = F_2(e + 1)$ . For the hyperbola, the denominator of  $R_1$  vanishes at the angles  $\psi_1 = \pm \arccos(1/e)$ , corresponding to two lines parallel to the hyperbola asymptotes.

In the cartesian coordinates  $x, z$  (defined with respect to the origin  $O$  in the figure), the equations for the hyperbola and the ellipse are:

$$(e^2 - 1)z^2 - x^2 = a^2(e^2 - 1) \quad (\text{hyperbola})$$

$$(1 - e^2)z^2 + x^2 = a^2(1 - e^2) \quad (\text{ellipse})$$
(17.11.4)

The semi-major axes are  $b^2 = a^2(e^2 - 1)$  or  $a^2(1 - e^2)$ . Because of the constraints (17.11.2), the angles  $\psi_1, \psi_2$  are not independent of each other. For example, solving for  $\psi_2$  in terms of  $\psi_1$ , we have in the hyperbolic case:

$$\cos \psi_2 = \frac{e^2 \cos \psi_1 - 2e + \cos \psi_1}{e^2 - 2e \cos \psi_1 + 1}$$
(17.11.5)

This implies the additional relationship and the derivative:

$$\frac{1 + \cos \psi_2}{e \cos \psi_2 + 1} = \left( \frac{1 + \cos \psi_1}{e \cos \psi_1 - 1} \right) \left( \frac{e - 1}{e + 1} \right)$$

$$\frac{d\psi_2}{d\psi_1} = \frac{\sin \psi_1}{\sin \psi_2} \left( \frac{e \cos \psi_2 + 1}{e \cos \psi_1 - 1} \right)^2$$
(17.11.6)

The incident ray  $R_1$  reflects off the surface of either the hyperbola or the ellipse as though the surface is locally a perfect mirror, that is, the local normal bisects the angle between the incident and reflected rays. The angles of incidence and reflection  $\phi$  shown on the figures are given by:

$$\phi = \frac{\psi_1 + \psi_2}{2} \quad (\text{hyperbola})$$

$$\phi = \frac{\pi}{2} - \frac{\psi_1 + \psi_2}{2} \quad (\text{ellipse})$$
(17.11.7)

To determine the aperture field on the aperture plane passing through  $F_2$ , we equate the power within a solid angle  $d\Omega_1 = \sin \psi_1 d\psi_1 d\chi$  radiated from the feed, to the power reflected within the cone  $d\Omega_2 = \sin \psi_2 d\psi_2 d\chi$  from the hyperbola, to the power passing through the aperture  $dA = \rho d\rho d\chi$ :

$$dP = U_1(\psi_1, \chi) d\Omega_1 = U_2(\psi_2, \chi) d\Omega_2 = \frac{1}{2\eta} |E_a|^2 dA$$
(17.11.8)

where  $U_1$  is the radiation intensity of the feed, and  $U_2$  the intensity of the virtual feed. The second of Eqs. (17.11.8) may be solved as in Eq. (17.8.2) giving:

$$|E_a| = \frac{1}{2F} (1 + \cos \psi_2) \sqrt{2\eta U_2(\psi_2, \chi)}$$
(17.11.9)

where  $F$  is the focal length of the parabola. From the first of Eqs. (17.11.8), we find:

$$\sqrt{U_2} = \sqrt{U_1} \sqrt{\frac{\sin \psi_1 d\psi_1}{\sin \psi_2 d\psi_2}} = \sqrt{U_1} \frac{e \cos \psi_1 - 1}{e \cos \psi_2 + 1}$$
(17.11.10)

Inserting this into Eq. (17.11.9) and using Eqs. (17.11.6), we obtain:

$$|E_a| = \frac{1}{2F} \left( \frac{e - 1}{e + 1} \right) (1 + \cos \psi_1) \sqrt{2\eta U_1(\psi_1, \chi)}$$
(17.11.11)

Comparing with Eq. (17.8.2), we observe that this is equivalent to a *single* parabolic reflector with an effective focal length:

$$F_{\text{eff}} = F \frac{e + 1}{e - 1}$$
(17.11.12)

Thus, having a secondary reflector increases the focal length while providing a convenient location of the feed near the vertex of the parabola. Cassegrain antenna aperture efficiencies are typically of the order of 0.65-0.70.

### 17.12 Lens Antennas

Dielectric lens antennas convert the spherical wave from the feed into a plane wave exiting the lens. Fig. 17.12.1 shows two types of lenses, one with a hyperbolic and the other with elliptic profile.

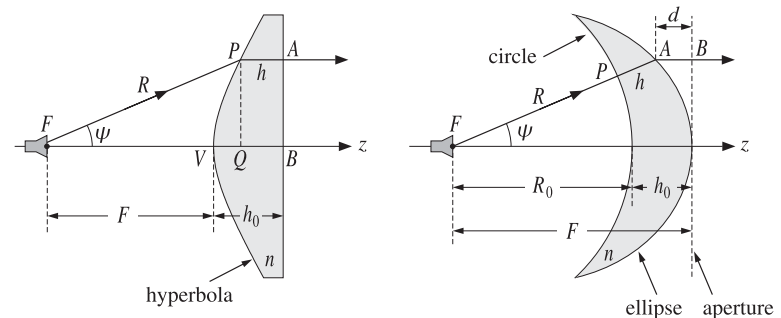


Fig. 17.12.1 Lens antennas.

The surface profile of the lens is determined by the requirement that the refracted rays all exit parallel to the lens axis. For example, for the lens shown on the left, the

effective aperture plane is the right side  $AB$  of the lens. If this is to be the exiting wavefront, then each point  $A$  must have the same phase, that is, the same *optical path length* from the feed.

Taking the refractive index of the lens dielectric to be  $n$ , and denoting by  $R$  and  $h$  the lengths  $FP$  and  $PA$ , the constant-phase condition implies that the optical length along  $FPA$  be the same as that for  $FVB$ , that is,

$$R + nh = F + nh_0 \quad (17.12.1)$$

But, geometrically we have  $R \cos \psi + h = F + h_0$ . Multiplying this by  $n$  and subtracting Eq. (17.12.1), we obtain the polar equation for the lens profile:

$$R(n \cos \psi - 1) = F(n - 1) \Rightarrow R = \frac{F(n - 1)}{n \cos \psi - 1} \quad (17.12.2)$$

This is recognized from Eq. (17.11.3) to be the equation for a hyperbola with eccentricity and focal length  $e = n$  and  $F_1 = F$ .

For the lens shown on the right, we assume the left surface is a circle of radius  $R_0$  and we wish to determine the profile of the exiting surface such that the aperture plane is again a constant-phase wavefront. We denote by  $R$  and  $h$  the lengths  $FA$  and  $PA$ . Then,  $R = R_0 + h$  and the constant-phase condition becomes:

$$R_0 + nh + d = R_0 + nh_0 \quad (17.12.3)$$

where the left-hand side represents the optical path  $FPAB$ . Geometrically, we have  $R \cos \psi + d = F$  and  $F = R_0 + h_0$ . Eliminating  $d$  and  $R_0$ , we find the lens profile:

$$R = \frac{F(1 - \frac{1}{n})}{1 - \frac{1}{n} \cos \psi} \quad (17.12.4)$$

which is recognized to be the equation for an ellipse with eccentricity and focal length  $e = 1/n$  and  $F_1 = F$ .

In the above discussion, we considered only the refracted rays through the dielectric and ignored the reflected waves. These can be minimized by appropriate antireflection coatings.

## 17.13 Problems

### 17.1 Cross Polarization.